MNRAS **000**, 1–25 (2020) Preprint 25 January 2021 Compiled using MNRAS LATEX style file v3.0

Stellar Migration and Chemical Enrichment in the Milky Way Disk: Predictions of a Hybrid Model

James W. Johnson,[1]★ David H. Weinberg,[1,2] Fiorenzo Vincenzo,[2] Jonathan C. Bird,[3] Sarah R. Loebman,[4] Alyson Brooks,[5] Thomas R. Quinn,[6] Charlotte R. Christensen,[7] et al.?

[1] *Department of Astronomy, The Ohio State University, 140 W. 18th Ave., Columbus, OH, 43210, USA*
[2] *Center for Cosmology and Astroparticle Physics (CCAPP), The Ohio State University, 191 W. Woodruff Ave, Columbus, OH, 43210, USA*
[3] *Department of Physics & Astronomy, Vanderbilt University, 2301 Vanderbilt Place, Nashville, TN, 37235, USA*
[4] *Department of Physics, University of California Merced, 5200 North Lake Rd., Merced, CA, 95343, USA*
[5] *Department of Physics & Astronomy, Rutgers University, 136 Frelinghuysen Rd, Piscataway, NJ, 08854, USA*
[6] *Department of Astronomy, University of Washinton, Box 351580, Seattle, WA, 98195, USA*
[7] *Department of Physics, Grinnell College, 1116 8th Ave., Grinnell, IA, 50112, USA*

Accepted XXX; Received YYY; in original form ZZZ

ABSTRACT

We investigate the impact of stellar migration on galactic chemical evolution models, considering a handful of assumptions for the star formation history and time-dependence of radial migration based on a zoom-in, hydrodynamical simulation of galaxy evolution. We find that models for the time-dependence of radial migration impact the type Ia supernova rate as a function of both time and radius, inducing significant variability. We demonstrate that this is a means with which young, α-enhanced stars can arise naturally out of inside-out galaxy growth with stellar migration. We find that the observed age-[α/Fe] relation is well-fit by an inside-out star formation history, while the age-[O/H] and age-[Fe/H] relations are well-fit by a late starburst model; no one model investigated here fits both simultaneously. Our model successfully reproduces the broad nature of the [α/Fe] distribution at fixed [Fe/H] in a given Galactic region; however, an overprediction of the frequency of intermediate [α/Fe] stars prevents it from explaining the observed results in detail. This suggests that inside-out galaxy growth combined with radial migration, even with a late starburst, is not conducive to forming the infamous bimodality as it is observed. We postulate that more dramatic evolutionary scenarios (e.g. a two-infall model) may be necessary to describe the observed results. In conducting this analysis, we developed and made use of newly released features in the `Versatile Integrator for Chemical Evolution` (`VICE`) which are built to handle these simulations under a wide variety of assumptions. `VICE` is publicly available at `https://pypi.org/project/vice`.

Key words: methods: numerical – galaxies: abundances, evolution, star formation, stellar content

1 INTRODUCTION

• Known for some time that stars undergo radial migration (e.g. Wielen et al. 1996); this is an effect which could considerably impact chemical evolution in galaxies by mixing stars that formed in different galactic regions with significantly different enrichment histories.

• To date there are only a handful of models which attempt to include this information, all focused on the Milky Way (e.g. Matteucci & Francois 1989; Schönrich & Binney 2009; Minchev et al. 2013; Sharma et al. 2020). Each of these studies treated the Milky Way as a series of concentric annuli, each described by a conventional one-zone model with parameters that change from annulus to annulus. In the resultant "multi-zone" model, stars and gas migrate between zones under some prescription to account for mixing processes. In this paper, we adopt an approach similar to that used by Minchev et al. (2013), in which the mixing processes are informed by star particles from a hydrodynamical simulation ran from cosmological initial conditions. With parameters tuned to reproduce observed results, such as abundance and surface density gradients, we can then assess the model predictions to address the following question: when combining simple, conventional assumptions about the star formation and dynamical histories of the Milky Way, what observed results can be replicated?

★ Contanct e-mail: johnson.7419@osu.edu

- The observables that we focus on are:
  - Metallicity distributions and abundance gradients
  - The [α/Fe] bimodality
  - The age-metallicty relation (AMR)
  - The young, α-rich population

- Metallicity Distributions and the Abundance Gradient

– Known for some time that the inner regions of Milky Way-like spirals are more metal-rich than their outskirts (SDSS references: Nordström et al. 2004b; Daflon et al. 2009; Frinchaboy et al. 2013; Hayden et al. 2014). There are variations depending on what type of stars are considered and what metallicity tracers are used. This qualitative result is also seen in the gas-phase (see, e.g., the results from the CHAOS project using HII regions; Berg et al. 2015, 2020).

– We know from APOGEE data that the observed MDF has a metal-poor mode and is skew-positive in the outer galaxy (and conversely, metal-rich and skew-negative in the inner galaxy; Hayden et al. 2015). The variation with Galactocentric radius is usually attributed to radial migration of metal-poor (metal-rich) stars from larger (smaller) radii, the same argument that (Sellwood & Binney 2002) used to interpret the results of Edvardsson et al. (1993) on the observed AMR in the solar neighborhood.

– Abundance gradients have been the focus of many studies and are quantified rather extensively, but their origin is somewhat up for debate. Applying the analytic models of Weinberg et al. (2017), one could argue that the gradient arises out of variations in the local gas-phase equilibrium abundance as a function of Galactocentric radius. This could be due to variations in the efficiency of outfowing winds removing metals from the star forming reservoir due to a deeper gravitational potential in the inner regions of Milky Way-like spirals. Nidever et al. (2014) used this methodology to successfully reproduce the APOGEE abundance data. However, recent chemical evolution models have successfully replicated the gradient with no outflowing winds at all (e.g. Minchev et al. 2013; Spitoni et al. 2019). This is based on arguments from Melioli et al. (2008, 2009) and Spitoni et al. (2008, 2009), who studied Galactic fountains and found that ejected metals tend to reaccrete to a Galactocentric radius similar to where they originated. With this result, some authors argue that such outflows do not significantly alter the chemical evolution of a Galactic disc. A notable difference between these two models is that the latter requires significantly lower nucleosynthetic yields to predict physically realistic abundances.

- The [α/Fe] bimodality

– Milky Way stars segregate themselves into the low- and high-α sequences, a bimodality found in, e.g., Gaia ESO (Recio-Blanco et al. 2014; Rojas-Arriagada et al. 2017), and APOGEE (Nidever et al. 2014; Hayden et al. 2015; Weinberg et al. 2019).

– Presence is well established, though origin a topic of intense debate.

– Notion that it could arise out of radial migration traces back to Schönrich & Binney (2009).

– Weinberg et al. (2017) models suggest increase in strength of the mass-loading factor η at late times would lower the equilibrium abundance, forming stars along the low-α sequence. This plus radial migration is yet unexplored.

– Spitoni et al. (2019, 2020) demonstrate that two-infall models can reproduce solar annulus data with good agreement. Recently, Spitoni et al. (2021) argued that this extends to other regions of the Galactic disc by reproducing APOGEE DR16 abundances by means of a chemical evolution model with three annuli centered on 4, 8, and 12 kpc. Although they're able to reproduce the data for different regions of the Galaxy, their model does not include a treatment for the migration of stars beyond their birth radius; though with 4-kpc annuli, it's not likely there would be much impact given the coarse nature of the binning.

– Grand et al. (2018) find with Auriga (Grand et al. 2017) that early, accretion induced starburst populates the high-α sequence, followed by low-level, sustained star formation on low-α sequence, and a rapid transition between the two ensures chemical space relatively unpopulated. This would imply short $\tau_\star$ (see justification in Weinberg et al. 2017). Ongoing, low-metallicity gas accretion can also populate low-α sequence. Buck (2020) find results qualitatively similar to second scenario in NIHAO simulation suite (Wang et al. 2015; Buck et al. 2020). Hydrodynamical simulations take into account radial migration by construction.

– Clarke et al. (2019) show that star formation proceeded in clumps in an SPH simulation of an NFW halo using GASOLINE (Navarro et al. 1997; Wadsley et al. 2017). The clumps self-enrich, forming stars on the high-α sequence, while more spatially extended, smooth star formation populated the low-α sequence.

– No shortage of models that reproduce the dichotomy, yet only those done with hydrodynamical simulations and a handful of others have taken into account radial migration.

- The Age-Metallicity Relation (AMR)

– Age-metallicity relation in the solar neighbourhood exhibits considerable intrinsic scatter (Edvardsson et al. 1993), usually attributed to radial migration of metal-rich (metal-poor) stars formed at smaller (larger) Galactocentric radii (Sellwood & Binney 2002; Haywood 2008; Roškar et al. 2008b; Schönrich & Binney 2009).

– Feuillet et al. (2018) reveal that super-solar metallicity stars are statistically older than solar metallicity stars (their Fig. 3). Contrasts with simple one-zone models where enrichment proceeds alongside star formation yielding a monotonic AMR (e.g. Andrews et al. 2017; Weinberg et al. 2017). One-zone models of starbursts can produce non-monotonic AMR due to the effect of dilution (Johnson & Weinberg 2020), but they by construction do not predict multiple abundances at fixed age. Argued using the Weinberg et al. (2017) analytic models that this is a consequence of radial migration - for a smooth star formation history (SFH), the youngest stars at any given radius will have composition reflective of the local equilibrium abundance, and only older stars will have had adequate time to migrate to a similar Galactocentric radius.

- The Young Alpha-Rich Population

– Population of young (~few Gyr), [α/Fe] ~ 0.1-0.2 stars in the solar neighbourhood.

– Found using stellar ages estimated from carbon-to-nitrogen ratios (Martig et al. 2016), isochrone matching (Feuillet et al. 2018, 2019), and with the asteroseismic ages in the original APOKASC catalog (Chiappini et al. 2015; Silva Aguirre et al. 2018; Pinsonneault et al. 2014). Silva Aguirre et al. (2018) demonstrated that these stars have kinematics similar to the rest of the high-α population, and argued based on this that they may be the consequence of stellar mergers or mass transfer events, making truly old stars simply appear younger.

– Mor et al. (2019) infer a factor of ∼2 enhancement in the SFH of the Milky Way ∼2 Gyr ago by comparing population synthesis models to observed stellar luminosity functions and color-magnitude diagrams from Gaia data (Gaia Collaboration et al. 2018). Isern (2019) reach similar conclusions by modeling the white dwarf luminosity function in the solar neighbourhood with Gaia parallaxes. Motivated by these results, Johnson & Weinberg (2020) demonstrate using one-zone chemical evolution models that a recent starburst can produce young, α-enhanced stars. Caveat: burst would have had to be sufficiently localized such that the young, α-rich stars remain outliers from an otherwise monotonically descreasing age-[α/Fe] relation.

· The impact of such evolutionary histories combined with a model for stellar migration is, to our knowledge, yet unexplored in the literature.

• A viable model for the detailed enrichment history of the Milky Way would explain simultaneously all of these observed results and their variations in different Galactic regions, while also taking into account effects like mixing and observational systematics. In this paper, we aim to assess the extent to which conventional assumptions about the evolutionary history of the Milky Way can account for these results, entertaining a handful of models describing the star formation history and time-dependence of radial migration.

– Motivated by the general result that Galaxies grow in radius (i.e. "inside-out" growth; Bird et al. 2013), our base-line model has a star formation history whose e-folding timescales grow with Galactocentric radius. Motivated by the findings of Mor et al. (2019) and Isern (2019), we also construct models which exhibit a recent enhancement in the star formation rate. For comparison, we also construct a model in which the SFH is constant with time at fixed radius; this is interesting primarily from a theoretical perspective, removing the effects of a time-varying SFH to quantify only what is predicted by ongoing star formation with radial mixing.

– While we make use of a hydrodynamical simulation to include the effects of radial migration, we do *not* make use of its star formation history. While Minchev et al. (2013) also made use of a hydrodynamical simulation in their study, ours differs from theirs in this key aspect. The Schönrich & Binney (2009) and Sharma et al. (2020) studies, on the other hand, chose a model for radial migration that was based on dynamical arguments, which introduced free parameters that then required fitting to data. An advantage of our decision to make use of a hydrodynamical simulation over dynamical arguments is that it's unclear the extent to which fitting to observed data biases the model into agreement with parts of the data that weren't part of the fit. A hydrodynamical simulation, while still an approximation of reality, is motivated by first principles in that it models the gravitational interactions of star particles with gas and other star particles as well as the diffuse dark matter halo. The primary disadvantage of this choice is a consequence of the lack of free parameters - the model is rigid, and we cannot explore slight variations. However, in principle one could compare the predictions made by our chemical evolution models but with different hydrodynamical simulations.

2 METHODS

• To fulfill the goals of this paper, we develop and make use of newly released features within the `Versatile Integrator for Chemical Evolution` (`VICE`), which are designed to handle these kinds of simulation with a wide range of flexibility. We reserve description of `VICE`'s algorithm and our simulation parameters for § 2.2, first describing our sample of star particles from the hydrodynamical simulation.

• We emphasize that the star particles from the hydrodynamical simulation are used *only* in the mixing component of our models. We make use of neither its star formation nor chemical enrichment histories; rather, these are exactly what we explore variations of in this paper. There is no N-body integration involved in our models.

2.1 The Hydrodynamical Simulation

• In this paper we make use of star particles from the `h277` simulation (Christensen et al. 2012; Zolotov et al. 2012; Loebman et al. 2012, 2014; Brooks & Zolotov 2014). A synopsis of the detailed simulation parameters and cosmological model can be found in § 2 of Bird et al. (2020). We do not go into detail on that here, instead focusing on how we vet the sample of star particles for use in our chemical evolution models.

• Of particular importance to have accurately measured formation radii for each star particle that we use in our analysis. `h277` did not record the exact birth radius of each star particle; however, each star particle does have an accurate age at each snapshot. If a star particle is sufficiently young in the first snapshot it appears in, then its radius in that snapshot is a reasonable approximation for its birth radius, since its orbit is unlikely to have changed significantly in a short enough time interval. Therefore, we restrict our sample to those with an age at first snapshot of $\leq$ 150 Myr, and adopt their Galactocentric radius at first snapshot as the birth radius. Also conducted the analysis with age at first snapshot of $\leq$50 Myr, and found similar results, suggesting this choice does not impact our conclusions. In practice, we find that 150 Myr also provides us with an adequately large number of star particles to sample from.

• Of the star particles with ages at first snapshot of $\leq$ 150 Myr, the oldest star is 12.26 Gyr old at the present day. Since `h277` ran for 13.7 Gyr, we therefore subtract 1.5 Gyr from the formation times of all star particles, and run our disc models for 12.2 Gyr. This value of T = 1.5 Gyr is likely tied to the onset of star formation in the `h277` disc, which would have occurred some time following the cosmological initial conditions at a lookback time of 13.7 Gyr. As a result, our disc models trace the chemical evolution of the Milky Way out to a lookback time of 12.2 Gyr, or a redshift of $z \approx 3$.

• We further restrict the sample of star particles to only those with both formation and final radii of $R_{\rm gal} \leq 20$ kpc, and to have formed within $|z| \leq 3$ kpc of the disc midplane. These criteria ensure that we're only using star particles which formed in-situ. While it's possible that some star particles formed in a dwarf galaxy as it was infalling which would satisfy these criteria, these star particles are small in number, and are only relevant at large $R_{\rm gal}$ and high ages, a region of parameter space where few stars form anyway.

• Based on a kinematic decomposition performed on the present-day phase space distribution of the `h277` star particles, we include all stars with bulge, pseudobulge, and disc-like kinematics, excluding the halo stars. While we're not modeling the evolution of the bulge here, these star particles are overwhelmingly located at $R_{\rm gal} \leq 3$ kpc at the present day anyway, while we're interested in $R_{\rm gal} \geq 3$ kpc in this paper since we're modeling the disc. This yields a sample of 3,000,556 star particles from `h277`.

• `h277` had a transient bar during its evolution, but does not have a bar at $z = 0$. The Minchev et al. (2013) model, and by extension the Minchev et al. (2014) and Minchev et al. (2017) models as

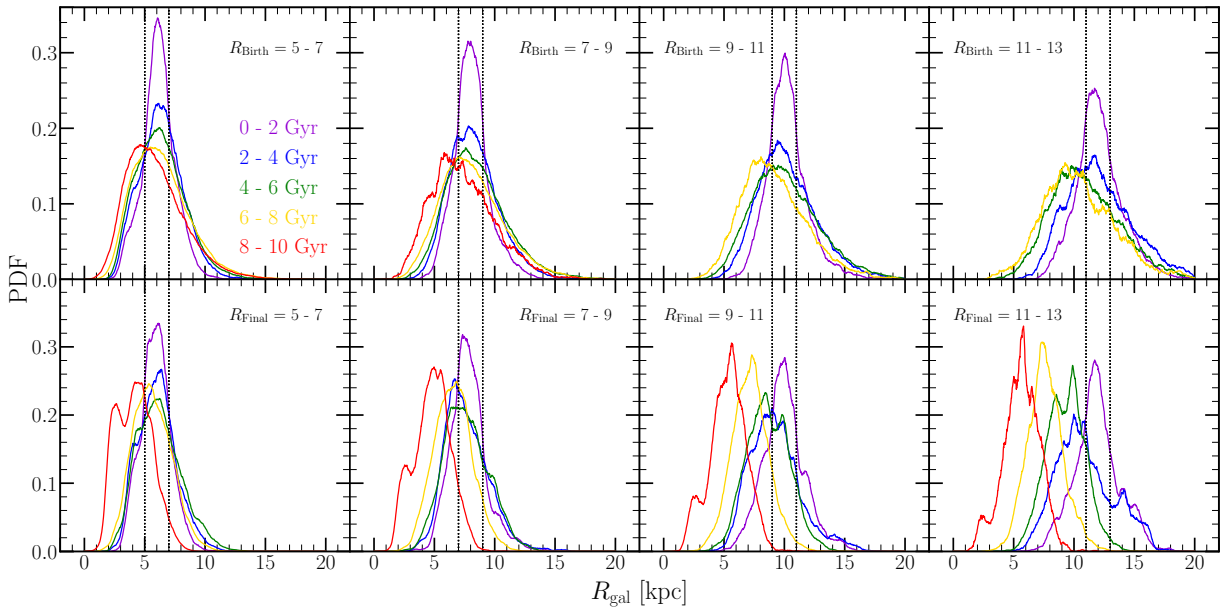

Figure 1. Radial distributions of our candidate analog star particles from `h277`. In the top row, we show distributions of *final* radius in bins of birth radius and age. In the bottom row, we show distributions of *birth* radius in bins of final radius and age. Each bin in Galactocentric radius is shown in its own panel, denoted in text at the top of each panel and by vertical black dashed lines. We color-code the distributions according to the age of the star particles, denoted by the legend in the upper left panel. We smooth all distributions with a box-car width of 0.5 kpc to improve clarity. We omit the distributions for 8 - 10 Gyr old stars born in the 9 - 11 and 11 - 13 kpc bins due to an insufficient number of star particles with which to calculate the distribution.

well, selected a hydrodynamical simulation specifically so that it would have a bar at $z = 0$. This could mean that the dynamical history of our models Galaxies do not reflect that of the Minchev et al. (2013) model, and perhaps the Milky Way itself. A detailed investigation on the impact of bar evolution on stellar migration and thus chemical evolution is outside the scope of this paper, though can be conducted in principle by simply swapping the `h277` data within `VICE` for another simulation, then rerunning our numerical models and comparing the results.

• Distributions of final radii in bins of birth radii and age are shown in the top row of Fig. 1. Conversely, the bottom row shows distributions of birth radii in bins of final radii and age.

– Focusing on the top row of panels in Fig. 1, we note that for stars born at any radius and time, the distribution of final radii is still peaked near the birth radius. With increasing age, it appears the mode final radius may move slightly inward. The tails of the distributions to large radii are relatively age-independent - some differences between the 0 - 2 and 8 - 10 Gyr age bins, but not much. However, the tails of the distributions to small radii are not age-independent, and move toward smaller $R_{\rm gal}$ with increasing age. This suggests that radial migration inward and outward occur on different timescales, in particular that inward migration is slower than outward migration. By extension this may suggest that inward and outward migration are tied to different physical processes. Roškar et al. (2008a) demonstrate using a cosmological simulation that resonant scattering at corotation causes stars to move outward and gas to move inward. It's possible that radial migration inward has different origins.

– Focusing on the bottom row of panels in Fig. 1, we note that the oldest stars at any Galactocentric radius at the present day were overwhelmingly born at smaller radii. The youngest stars, however, were overwhelmingly born at comparable radii, and the stars of intermediate ages simply span the range in radii between the two. With increasing radius, the differences in the mode of the birth radius distribution between age bins gets larger.

– The differences in distributions shown in the top and bottom panels boils down to stellar surface density being a strong function of Galactocentric radius. Take for example the age = 8 - 10 Gyr bin in both $R_{\rm Birth}$ = 5 - 7 kpc and $R_{\rm Final}$ = 11 - 13 kpc bins (i.e. the red curves in the top-left and bottom-right panels). For these old stars born at 5 - 7 kpc, 11 - 13 kpc is far down the tail of the $R_{\rm Final}$ distribution, and yet 5 - 7 kpc is the mode $R_{\rm Birth}$ of all old stars presently at these radii. This implies that even though the majority of 8 - 10 Gyr old stars with $R_{\rm Final}$ = 11 - 13 kpc were born at 5 - 7 kpc, they make up only a small fraction of the stars with similar birth radii. This is only possible if the stellar surface density gradient is sufficiently steep, which it is known to be (e.g. Bland-Hawthorn & Gerhard 2016).

· Fig. 1 also demonstrates that the numbers of stars that migrated inward and outward are comparable in `h277`. Taking a $|\Delta R_{\rm gal}| \geq 500$ pc between birth and final radii as the criterion for migrating inward or outward, indeed we find that in our sample, 27% migrated inward, 29% migrated outward, and the remaining 44% stayed near their birth radius. These are global percentages.

– In all bins of birth radius, a good first-order estimate of the probability density that a star has a final radius in the same bin is ~0.3. With bins in radius on this plot of 2 kpc, this suggests that ~40% of stars migrate significantly by the time they're ~2 Gyr old. If the SN Ia DTD is a $t^{-1.1} \approx t^{-1}$ power-law as suggested by recent observations (e.g. Maoz & Mannucci 2012; Maoz & Graur 2017), then we expect similar numbers of SN Ia events to occur with delay times between 1 and 10 Gyr as we do between 100 Myr and 1 Gyr. With such an extended DTD, and the distributions in final radius shown in the bottom panel of Fig. 1, its possible that white dwarfs migrate significant distances before

producing a SN Ia event. Indeed, in the ASAS-SN bright supernova catalog, ~10% of supernovae are seen at >10 kpc from their host galaxies (Holoien et al. 2019). While this catalog is for *all* supernovae, the majority of SN events are type Ia anyway. Based on this, it's reasonable to expect that the migration of nucleosynthetic yields may proceed alongside stellar migration, an effect which is often neglected (e.g. Minchev et al. 2013, and the application of the Weinberg et al. 2017 analytic models in Feuillet et al. 2018). In this paper, we relax this assumption. The application of the `h277` star particle data to our model for radial migration and the time dependence thereof is discussed in the next section.

2.2 Radial Migration

• To simulate our models, we develop and make use of `VICE`'s `milkyway` object, an extension of a more general object named `multizone`. The `multizone` object is at its core an array of `singlezone` objects, which are designed to handle simulations of one-zone models and were the focus of Johnson & Weinberg (2020), `VICE`'s initial release paper. The `multizone` object then affords the user the ability to move gas between zones with any given time dependence, and to assign all stellar populations any given zone at any given time following their birth, effectively allowing arbitrarily complex zone and migration schema. The `milkyway` object is a user-friendly extension of this which enforces a zone configuration in which the Galaxy is modeled as a series of concentric annuli of uniform width $\Delta R_{\rm gal}$. As defaults, it adopts the stellar migration model described in this section and our star formation law described in § 2.5.

• Stars in `VICE` are stand-ins for entire stellar populations, and in the `milkyway` object, are said to be in a given zone/annulus if their radius is between the inner and outer edges. At all times, their nucleosynthetic products and returned envelopes are placed in the ISM of the annulus that they are in *at that time*.

• Where hydrodynamical and N-body simulations of galaxy evolution often use star particles of a fixed mass, `VICE` forms a fixed number of stellar populations in a given zone at a given timestep, and allows their masses to vary to account for variations in the star formation rate. The mass of stars formed in a given zone is divided evenly among the stellar populations that form during a given timestep.

• Algorithm based on initial and final radii of star particles in hydrodynamical simulations, for which we've taken `h277` as discussed in the previous section.

• In modeling the Milky Way as a series of concentric annuli, `VICE`'s `milkyway` object assumes stellar populations to be born at the centres of each annulus. For a stellar population born at a time T and Galactocentric radius $R_{\rm gal}$, it first searches for star particles from `h277` that formed at $T\pm$ 250 Myr and $R_{\rm gal}\pm$ 250 pc. It then randomly selects a star particle from this subsample with no bias to act as an *analog*. This stellar population then assumes the change in orbital radius $\Delta R_{\rm gal}$ of its analog at face value, and moves from its birth radius to the implied final radius at T = 12.2 Gyr with some time dependence. If no candidate analogs are found, `VICE` widens the search to $T\pm$ 500 Myr and $R_{\rm gal}\pm$ 500 pc. While the maximum allowed difference in birth times caps here at 500 Myr, we allow the difference in birth radii to continue increasing by 250 pc until a candidate analog is found.

– In principle this allows stellar populations to be assigned analogs with significantly different birth radii; however, this is only an issue for small T and large $R_{\rm gal}$ where there are few star particles from `h277`, and where few stars form in nature anyway due to the inside-out growth of Galaxies. Furthermore, due to the similarity of the histograms in the top row of Fig. 1, we expect taking $\Delta R_{\rm gal}$ from a star particle which formed at a similar time but different birth radius in these instances to be accurate enough for our purposes.

– Each annulus in our models does not contain any vertical information; that is, the displacements of stars from the disc midplane $|z|$ does not enter into our models at all. After running a `VICE` simulation, each stellar population is simply assumed to be located at the present-day $z_{\rm final}$ of its assigned analog. In effect, this retains the assumption that the gas-phase abundances are verticaly and azimuthally well-mixed, and that changes in the gas composition at a given time happen only in the radial direction.

– When a star particle is assigned as an analog to a stellar population in our simulations, it is *not* thrown out of the sample of candidate analogs, in theory allowing a star particle to act as an analog for multiple stellar populations. This is a difference between the Minchev et al. (2013) model and ours. Where we assign star particles to stellar populations for which `VICE` then calculates a stellar mass and composition based on an assumed star formation history, the Minchev et al. (2013) model assigns compositions to star particles.

• Our migration models

– With our data from the `h277` simulation providing a stellar population born at some radius $R_{\rm gal}$ and time T with the required $\Delta R_{\rm gal}$, we construct the following four models describing the time-dependence with which a stellar population moves to its final radius.

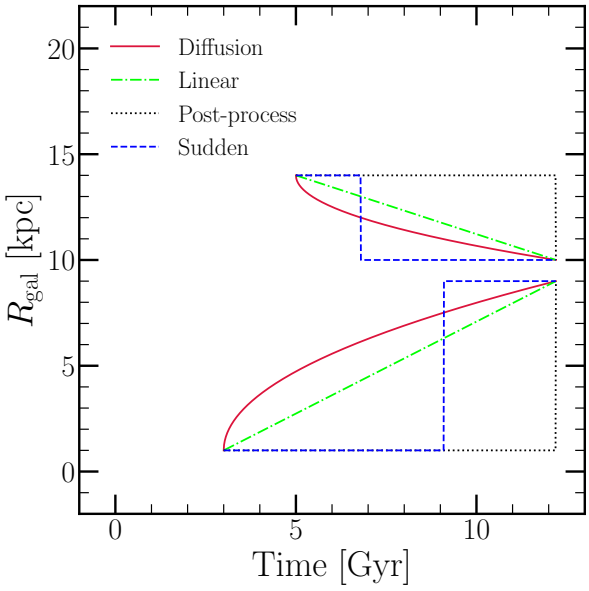

Figure 2. A diagram illustrating how Galactocentric radius changes with time for two stellar populations under our migration schema: diffusion (crimson, solid), linear (lime, dot-dashed), post-process (black, dotted), and sudden (blue, dashed). Here the initial and final radii and birth times are chosen at random for illustrative purposes. With the initial and final Galactocentric radii of a stellar population, its birth time, and one of these assumptions about the time-dependence of migration, the Galactocentric radius at all times is known.

– All models here neglect radial gas flows, this paper instead focusing on these simple models describing how orbital radii change with time. Investigation of our models with radial gas flows would be an interesting extension to this paper.

– **Post-processing**: Stars stay where they are born until the final timestep. Based on the assumption that stellar populations do not contribute to enrichment beyond their birth radius (e.g. Minchev et al. 2013). Each annulus simulated as a one-zone model independent of all other zones. Shown in black dotted line in Fig. 2.

– **Sudden**: A random number is drawn from a uniform distribution between the time of birth and the present day. That time is taken to be the time of instantaneous migration to the present-day annulus. Emulates a scenario in which a single dynamical interaction changes the orbital radius of a star. Can be thought of as a time-dependent extension of the post-processing scenario. Shown in blue dashed line in Fig. 2.

– **Diffusion**: A case in which stars migrate in a continuous, time-dependent manner. If stars move to their final radii via a random walk, then the mean displacement of stars that migrate similar distances would scale with $\sqrt{\text{age}}$. This is shown in the red solid line in Fig. 2. This is our fiducial migration model; we present results using this model except where otherwise noted. It is so named because it corresponds to a scenario in which the random walk carries out the diffusion of angular momentum. This is qualitatively similar to Frankel et al. (2018, 2020), who also model radial orbit migration with a $\sqrt{\tau}$ dependence.

– **Linear**: A simple variation of the diffusion model. Has no physical motivation other than numerical ease, but together with the diffusion model constitutes a test of how sensitive our models are to the assumed time-dependence of stellar migration. Demonstrated by green dot-dashed line in Fig. 2.

• Further details on the implementation of the `milkyway` object, the more general `multizone` object, and other features of `VICE` can found in its documentation. [1]

• We have a sample of 3,000,556 candidate analog star particles from `h277`, only ~57% of which are disc stars. Since we're modeling the thin and thick disc populations here, ~1.71 million is a much better estimate of the number of analogs that we can realistically sample from. We take $\Delta R_{\rm gal}$ = 100 pc as the width of each annulus from $R_{\rm gal}$ = 0 to 20 kpc and a timestep size of ΔT = 10 Myr from T = 0 to 12.2 Gyr (see discussion in §2.1 for our choice of time-interval). With the resulting 200 zones and 1,221 timesteps, we let `VICE` from n = 9 stellar populations per zone per timestep, resulting in 2,197,800 total stellar populations with predicted masses and abundances. While this is more than the number of disc particles in our sample of candidate analogs, we force the star formation rate to zero beyond $R_{\rm gal}$ = 15.5 kpc; while these stellar populations exist within `VICE` and are a part of the computational overhead, they have zero mass and thus do not contribute to the chemical evolution. This results in 1,692,306 stellar populations with *non-zero* masses and abundances predicted by `VICE`, reasonably within the limit of what we can sample. These simulations run in ~6 hours and take up ~235 MB of disc space per output, including the extra data that we record for each stellar population's analog star particle.

• We emphasize that `h277` provides our model with *only* the $\Delta R_{\rm gal}$ and $z_{\rm final}$ for each individual stellar population. We do not use the SFH of `h277` or its chemical enrichment history in any way, making use of only the dynamical history. There is no N-body algorithm embedded within `VICE` determining the positions of stars at times between their birth and the present day.

[1] https://vice-astro.readthedocs.io

2.3 Nucleosynthetic Yields, Outflows, and Recycling

• *Fractional net* yields, as required by `VICE`. Recycling is implemented separately, such that stellar envelopes are returned to the ISM at the birth composition of each stellar population. `VICE` takes the general approach of returning previously produced material according to a stellar lifetime model and injecting newly produced nucleosynthetic products as described below. Also clarify that these are not *effective* yields in that outflows are also implemented separately.

• CCSN events are assumed to occur immediately following the formation of their progenitor stars. This is an adequate approximation, because the lifetimes of massive stars are short compared to the relevant timescales for galaxy evolution. For the most massive stars, the lifetimes are comparable to the timestep size that we take use in these simulations anyway. This assumption implies a linear relationship between CCSN enrichment and the star formation rate:

$$\dot{M}_x^{\rm CC} = y_x^{\rm CC}\dot{M}_\star \tag{1}$$

– Physically, the CCSN yield $y_x^{\rm CC}$ is the fraction of a stellar population's initial mass that is converted into some element x and ejected to the ISM, neglecting outflows.

– Take $y_{\rm O}^{\rm CC} = 0.015$ and $y_{\rm Fe}^{\rm CC} = 0.0012$ from Johnson & Weinberg (2020), who in turn adopt these values from Weinberg et al. (2017).

• SN Ia products injected with a $t^{-1.1}$ delay-time distribution (DTD) with a minimum delay-time of $t_{\rm D}$ = 150 Myr. This is the default DTD in `VICE`, adopted in Johnson & Weinberg (2020), and is suggested by recent observational results comparing the cosmic SN Ia rate to the cosmic SFH (Maoz & Mannucci 2012; Maoz & Graur 2017). In a one-zone model at times $t > t_{\rm D}$, the enrichment rate for some element x can be expressed as the product of some yield $y_x^{\rm Ia}$ and the star formation history weighted by the DTD:

$$\dot{M}_x^{\rm Fe} = y_x^{\rm Fe}\langle\dot{M}_\star\rangle_{\rm Ia} \tag{2a}$$

$$= y_x^{\rm Fe}\frac{\int_0^{t-t_{\rm D}}\dot{M}_\star(t')R_{\rm Ia}(t-t')dt'}{\int_{t_{\rm D}}^{t_{\rm max}}R_{\rm Ia}(t-t')dt'} \tag{2b}$$

where $R_{\rm Ia}$ is the DTD itself, in units of $\rm M_\odot^{-1}\ Gyr^{-1}$. Like the CCSN yield, $y_x^{\rm Ia}$ is simply the fraction of a single stellar population's mass that is converted into the element x over the ensuing SN Ia duty cycle. It can also be expressed as an integral over the DTD:

$$y_x^{\rm Ia} = m_x^{\rm Ia}\int_{t_{\rm D}}^{t_{\rm max}}R_{\rm Ia}(t)dt = m_x^{\rm Ia}\frac{N_{\rm Ia}}{M_\star} \tag{3}$$

where the $m_x^{\rm Ia}$ is the mass of some element x produced in a single SN Ia event on average, and the integral evaluates to the mean number of Ia events $N_{\rm Ia}$ per mass of stars formed $M_\star$.

– `VICE` enforces $t_{\rm max}$ = 15 Gyr always, though provided one is consistent with equations (3) and (2b), the results are independent of $t_{\rm max}$ since the integrals cancel.

– Extending this to multi-zone models is simple - rather than an integral over the star formation history of a given annulus, the

rate becomes a summation over all stellar populations that are in a given zone at some time:

$$\dot{M}_x^{\rm Ia} = y_x^{\rm Ia} \frac{\sum_i M_i R_{\rm Ia}(\tau_i)}{\int_{t_{\rm D}}^{t_{\rm max}} R_{\rm Ia}(t) dt} \quad (4)$$

where M_i and τ_i are the mass and age of the i'th stellar population, respectively.

– Initially adopt $y_{\rm O}^{\rm Ia} = 0$ and $y_{\rm Fe}^{\rm Ia} = 0.0017$ from Johnson & Weinberg (2020) and Weinberg et al. (2017). However, in practice we find that the e-folding timescales of star formation in our models are sufficiently long (see discussion in § 2.4) such that our fiducial, inside-out SFH model predicts [O/Fe] ≈ +0.05 for young stars. We therefore multiply this value by a factor of $10^{0.1}$, adopting instead $y_{\rm Fe}^{\rm Ia} = 0.00214$ so that our fiducial model predicts a late-time [O/Fe] ratio in better agreement with observations. This change is likely within the uncertainties in nucleosynthetic yields anyway.

– Our model assumes that all supernova yields of O and Fe are independent of metallicity. While this appears to be empirically true for CCSN yields of these elements (e.g. Weinberg et al. 2019; Griffith et al. 2020), recent evidence by Brown et al. (2019) suggests that the local specific SN Ia rate shows a strong, inverse dependence on galaxy stellar mass. They argue that this may imply a metallicity dependent $R_{\rm Ia}$ that produces more SN Ia events at early times when the metallicity is low. While we adopt a metallicity independent $y_{\rm Fe}^{\rm Ia}$ in this paper, `VICE` allows users to specify any functional form for $y_{\rm Fe}^{\rm Ia}$ as a function of the total abundance by mass Z, allowing future studies of the impact of this to proceed straight-forwardly.

• Our model assumes that all supernova yields of O and Fe are independent of metallicity. While this appears to be empirically true in the Milky Way (Weinberg et al. 2019; Griffith et al. 2020), our CCSN yields are based on supernova explosion models in which all >8 $M_\odot$ progenitor produces a CCSN event (e.g. Chieffi & Limongi 2004, 2013). Recent findings with regard to black hole formation and stellar explodability have demonstrated that many massive stars simply do not produce a supernova explosion (see theoretical discussion by, e.g., Pejcha & Thompson 2015; Sukhbold et al. 2016, and observational evidence from Gerke et al. 2015; Adams et al. 2017; Basinger et al. 2020). Such effects would necessarily lower CCSN yields of all elements. While `VICE` includes functionality with which to calculate $y_x^{\rm CC}$ for some element x using built-in tables from supernova nucleosynthesis studies, an in-depth investigation of the impact of these effects is outside the scope of this paper. Such an investigation which expands the capabilities of `VICE` will be presented in Griffith et al. (2021, in prep). With regard to our SN Ia yields, Brown et al. (2019) demonstrate that the local specific SN Ia rate shows a strong, inverse dependence on galaxy stellar mass. They argue that this may imply a metallicity dependent $R_{\rm Ia}$ that produces more SN Ia events at early times when the metallicity is low. However, these metallicities are only present in our models at very early times. Furthermore, when outflows are taken into account, these yields are known to predict observationally plausible abundances (Andrews et al. 2017; Weinberg et al. 2017).

• Weinberg et al. (2017) demonstrate that, to first order, the nucleosynthetic yields of a given element and the strength of outflowing winds determine the late-time equilibrium abundance in the ISM. We retain their characterization of outflows here, in terms of a mass-loading factor η:

$$\eta \equiv \frac{\dot{M}_{\rm out}}{\dot{M}_\star} \quad (5)$$

Here we adopt a scaling of η with $R_{\rm gal}$ such that the late-time equilibrium abundance as a function of radius describes a metallicity gradient in agreement with observations; a similar methodology was employed by Nidever et al. (2014).

• The procedure outlined in this section makes two assumptions: 1) that the equilibrium abundance at a given radius corresponds to the mode of the observed MDF, and 2) that radial migration does not significantly impact the overall form of the gradient. We demonstrate that this holds in our simulations in § 3.1.

• For α elements, Weinberg et al. (2017) defines the equilibrium abundance under a constant SFH as:

$$Z_{\alpha,\rm eq} = \frac{y_\alpha^{\rm CC}}{1 + \eta(R_{\rm gal}) - r} \quad (6)$$

where r is the recycling parameter (≈ 0.4 for the sake of this scaling with a Kroupa IMF; see discussion in their § 2.2). Solving for $\eta(R_{\rm gal})$ yields:

$$\eta(R_{\rm gal}) = \frac{y_\alpha^{\rm CC}}{Z_{\alpha,\rm eq}} + r - 1 = \frac{y_\alpha^{\rm CC}}{Z_{\alpha,\odot}} 10^{-\text{mode}([\alpha/\rm H])(R_{\rm gal})} + r - 1 \quad (7)$$

• A fundamental observable, the observed metallicity gradient in the Milky Way has been the focus of a considerable number of studies to date.

– Nordström et al. (2004b) find a gradient of -0.099 $\rm kpc^{-1}$ in [Fe/H] in main sequence stars from GCS (Nordström et al. 2004a; Holmberg et al. 2007).

– Daflon et al. (2009) find a gradient of -0.04 $\rm kpc^{-1}$ in [S/H] in OB stars

– Frinchaboy et al. (2013) find a gradient of -0.09 $\rm kpc^{-1}$ in [M/H] in open clusters.

– Hayden et al. (2014) also find -0.09 $\rm kpc^{-1}$ in [M/H] for $R_{\rm gal} \gtrsim 6$ kpc for low-α stars. For $R_{\rm gal} \lesssim 6$ kpc, they find a relatively flat gradient.

– Weinberg et al. (2019) finds -0.06 $\rm kpc^{-1}$ in mode([Mg/H]) for upper red giant branch disc stars (see their Fig. 23).

• We assume a slope of -0.08 $\rm kpc^{-1}$, in tentative agreement with the previous studies that quote the slope of the gradient mentioned above. To set the normalization, we assume the mode([α/H]) to be ∼+0.3 at $R_{\rm gal}$ = 4 kpc, since this would produce mode([α/H]) ≈ 0 at $R_{\rm gal} \approx$ 7 - 9 kpc. This results in the following form for η as a function of Galactocentric radius:

$$\eta(R_{\rm gal}) = \frac{y_\alpha^{\rm CC}}{Z_{\alpha,\odot}} 10^{(-0.08\ \rm kpc^{-1})(R_{\rm gal} - 4\ \rm kpc) + 0.3} + r - 1 \quad (8)$$

where we adopt our yield of O for $y_\alpha^{\rm CC}$ and the solar abundance of O of $Z_{\rm O,\odot} = 0.00572$ based on Asplund et al. (2009).

• This does assume a uniformly linear gradient at all $R_{\rm gal}$. Hayden et al. (2014) do find the gradient in [M/H] to flatten for $R_{\rm gal} \lesssim$ 6 kpc, challenging this assumption. However, this procedure can be easily repeated for any desired gradient, since the functional form simply goes into the power of 10 in equation (8).

• The top panel of Fig. 3 plots this scaling of η with $R_{\rm gal}$, highlighting a value of ∼2.15 for the solar circle in the red dotted line.

• Both AGB star enrichment and the recycling of previously produced nucleosynthetic material in this paper proceed as they did in Johnson & Weinberg (2020), with the caveat that the mass is

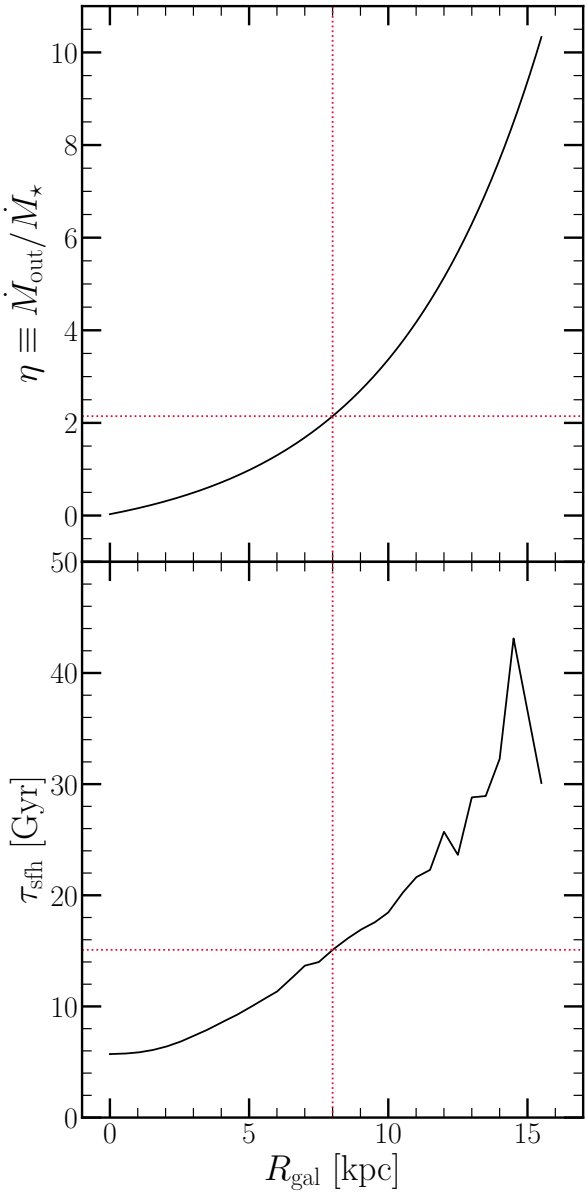

Figure 3. Top: Our implemented scaling of the mass loading factor η with Galactocentric radius (black) as defined by equation (8). **Bottom**: The e-folding timescales of the star formation histories of our model galaxies (black). These values come from a fit to the $\Sigma_\star$-age relation in bins of R/R_e for $10^{10.5}$ - 10^{11} $M_\odot$ Sa/Sb Hubble type spiral galaxies as reported by Sánchez (2020, see discussion in § 2.4). The horizontal and vertical red dashed lines in both panels highlight a mass loading factor of $\eta \approx 2.15$ and a star formation timescale of $\tau_{\rm sfh} \approx 15$ Gyr at an assumed radius of the sun of $R_\odot = 8$ kpc.

added to the annulus that a stellar population is in at a given time, which may or may not be the annulus it was born in. `VICE` in its current version forces an AGB enrichment channel in all models; for this reason, it is also included in our models here, for which we adopt the yields sampled on a table of initial stellar mass and metallicity from Cristallo et al. (2011). However, the AGB star yields of O and Fe are negligible compared to their supernova yields.

- While we make use of these new simulation features in `VICE` here, it includes a number of useful features not relevant to the current paper (e.g. CCSN yield calculations using built-in tables from supernova studies, z-dependent CCSN and SN Ia yields, user-constructed AGB yields as functions of stellar mass and metallicity, the exchange of gas between zones in a multi-zone model). Potentially move these statements to the conclusions section near the end, where it's already mentioned that `VICE` is publicly available.

2.4 Star Formation Histories

- `VICE`'s simulations runs in either infall, star formation, or gas mode, referring simply to which component of the evolutionary history the user has specified. The fiducial starburst models presented in Johnson & Weinberg (2020) ran in infall mode, but here we run things in star formation mode, since we are after specific forms for the star formation histories of our models. This means that changing our assumptions about the star formation law described in § 2.5 would not change the star formation rate, but would change the surface density of gas at each timestep, and thus also the implied infall rates.
- Appendix A presents justification of how we normalize the parameters of our star formation histories to produce a realistic model Galaxy at the end of the simulation. In short, it takes in a unitless description of the time-dependence of the SFH at a given Galactocentric radius, denoted $f(t|R_{\rm gal})$, and a unitless description of the radial dependence of the present-day stellar surface density, denoted $g(R_{\rm gal})$. In short, we integrate $f(t|R_{\rm gal})$ with time for each annulus, assuming $R_{\rm gal}$ to correspond to the centre of the zone, and attach a prefactor to $f(t|R_{\rm gal})$ at each $R_{\rm gal}$ such that the desired gradient is achieved with a total stellar mass similar to that of the Milky Way. This procedure neglects the impact of radial migration, assuming that it does not significantly alter the form of $g(R_{\rm gal})$. We demonstrate that these assumptions hold in §2.6, in which we also detail our adopted form of $g(R_{\rm gal})$. As long as this assumption is not violated, the equation derived in Appendix A can be used to normalize the parameters of future models of spiral galaxies.
- We present four fiducial SFHs, which we dub "constant", "inside-out", "late-burst", and "outer-burst". They're defined as follows:

  – **Constant**: The SFH at a given radius is time-independent.

$$f_{\rm C}(t|R_{\rm gal}) = 1 \tag{9}$$

This case is of particular theoretical interest because it quantifies the effect of ongoing with star formation with radial migration, and no additional effects.

  – **Inside-Out**:

$$f_{\rm IO}(t|R_{\rm gal}) = (1 - e^{-t/\tau_{\rm rise}})e^{-t/\tau_{\rm sfh}} \tag{10}$$

We adopt this scenario over the traditional linear-times-exponential form of $f(t|R_{\rm gal}) \sim te^{-t/\tau_{\rm sfh}}$, because the latter does not offer control over the position of the maximum. The form we adopt has a maximum near $\tau_{\rm rise}$, for which we adopt a value 2 Gyr everywhere in this paper. We find that this produces a peak in star formation at lookback times of ~10 Gyr, corresponding to a redshift of $z \approx 2$, which is around cosmic high noon. In this paper $\tau_{\rm sfh}$ is a function of $R_{\rm gal}$ here, and we discuss it briefly in a few paragraphs.

  – **Late-Burst**: An inside-out SFH with a gaussian describing a starburst.

$$f_{\rm LB}(t|R_{\rm gal}) = f_{\rm IO}(t|R_{\rm gal})(1 + A_{\rm b}e^{-(t-t_{\rm b})^2/2\sigma_{\rm b}^2}) \tag{11}$$

$A_{\rm b}$ is a dimensionless parameter describing the strength of the starburst, $t_{\rm b}$ is the time of the local maximum in the SFH during

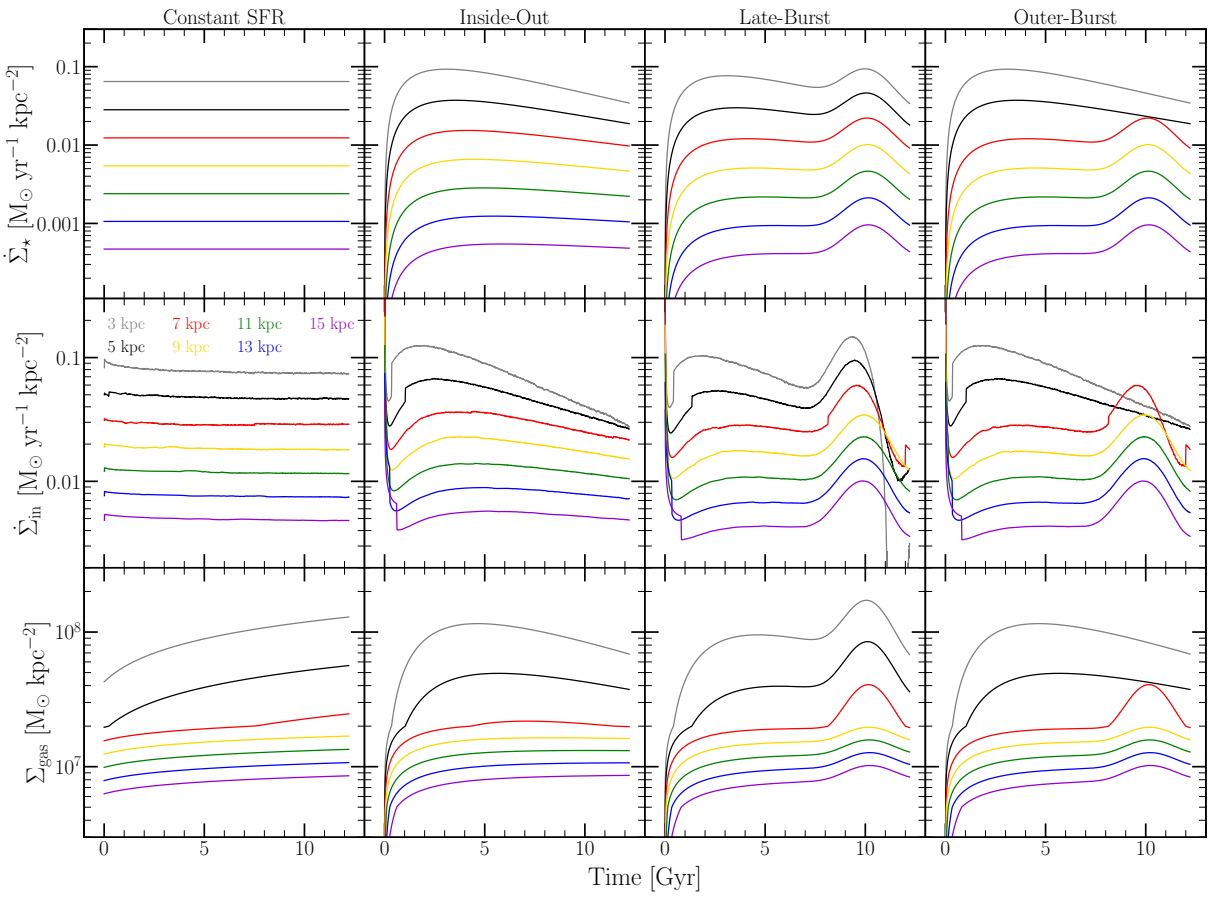

Figure 4. The surface densities of star formation $\dot{\Sigma}_\star$ (top row), infall $\dot{\Sigma}_{\rm in}$ (middle row), and gas $\Sigma_{\rm g}$ (bottom row) as functions of simulation time for our four fiducial SFHs: constant (far left), inside-out (left middle), late-burst (right-middle), and outer-burst (far right). We plot curves for the annuli whose inner radii are 3 kpc (grey), 5 kpc (black), 7 kpc (red), 9 kpc (yellow), 11 kpc (green), 13 kpc (blue), and 15 kpc (purple) (see equations (9), (10), (11), and (12) for the mathematical definition of each SFH).

the burst, and $\sigma_{\rm b}$ is the width of the gaussian describing it. Loosely motivated by the findings of Isern (2019) and Mor et al. (2019). Here we take $A_{\rm b}$ = 1.5, $t_{\rm b}$ = 10.2 Gyr, and $\sigma_{\rm b}$ = 1 Gyr.

– **Outer-Burst**: A variation of the late-burst model in which only $R_{\rm gal} \geq 6$ kpc experience the starburst. Loosely motivated by findings of Vincenzo & Kobayashi (2020) where a hydrodynamical simulation of a Milky Way-like galaxy showed radially dependent infall.

$$f_{\rm OB}(t|R_{\rm gal}) = \begin{cases} f_{\rm IO}(t|R_{\rm gal}) & (R_{\rm gal} < 6 \text{ kpc}) \\ f_{\rm LB}(t|R_{\rm gal}) & (R_{\rm gal} \geq 6 \text{ kpc}) \end{cases} \quad (12)$$

– Although we do not investigate it here, an investigation into the impact of more episodic star formation histories would be an interesting extension of this paper. For example, `VICE` has all of the necessary features to handle models in which major episodes of star formation coincide with the close passages of the Sagittarius dwarf (e.g. Ruiz-Lara et al. 2020).

• Derive e-folding timescales of star formation $\tau_{\rm sfh}$ from the data in Sánchez (2020).

– They present the stellar surface density $\Sigma_\star$ as a function of age in bins of $R/R_{\rm e}$ for MaNGA galaxies, where $R_{\rm e}$ is the half-light radius. They conduct this analysis in bins of stellar mass and for different Hubble types. Here take their $M_\star = 10^{10.5}$ - 10^{11} $M_\odot$ bin for Sa/Sb spirals (i.e. Milky Way-like galaxies).

– Their reported $\Sigma_\star$-age relation is not robust enough to get individual SFHs directly, but does allow the parameters of some fiducial mathematical model to be fit to the population-averaged trends. Assuming the $f_{\rm IO}(t|R_{\rm gal})$ form, we simultaneously fit the normalization and the e-folding timescale $\tau_{\rm sfh}$ to these data. Although the normalization is irrelevant to our simulations and determined via the method outlined in Appendix A, we adopt the resulting $\tau_{\rm sfh}$-$R_{\rm gal}$ relation in our models. Results are shown in Fig. 3.

– Note that the star formation timescales are long, even for the solar annulus ($\tau_{\rm sfh} \approx 15$ Gyr at $R_\odot = 8$ kpc) and especially for the outer galaxy. Beyond the solar annulus, SFHs are nearly constant after the initial rise at early times.

– With our adopted gradient (see §2.6, we know the present-day half-mass radius to be very near 4 kpc (this is just doing a couple integrals over the area of the disc). The findings of García-Benito et al. (2017) and González Delgado et al. (2014) suggest that half-light radii are marginally larger than half-mass radii. Based on equations (4) of González Delgado et al. (2014) relation the two for circular apertures, we expect our model galaxy to have a half-light radius near 5 kpc. We therefore adopt $R_{\rm e}$ = 5 kpc in calculating $\tau_{\rm sfh}$ as a function of radius. As I understand it,

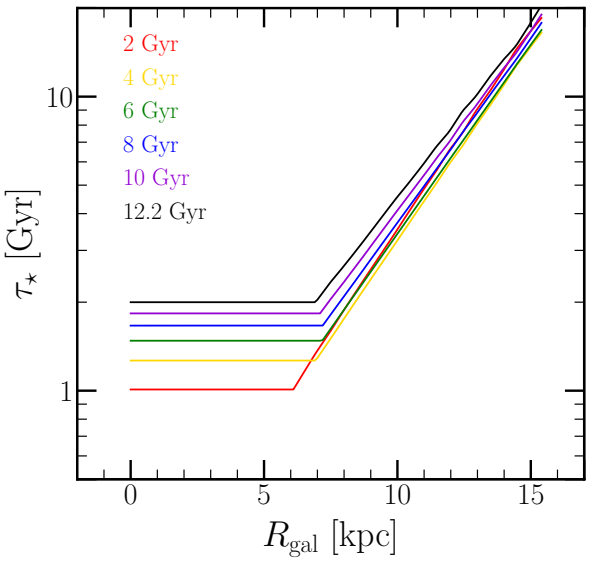

Figure 5. The star formation efficiency timescale $\tau_\star$ as a function of Galactocentric radius at simulation times of 2 Gyr (red), 4 Gyr (yellow), 6 Gyr (green), 8 Gyr (blue), 10 Gyr (purple), and 12.2 Gyr (i.e. the present day, black) predicted by our inside-out SFH model.

there are some results that suggest this value for the Milky Way as well?

• Given the assumed star formation histories, the gas supply at all times is known via the SFE timescale $\tau_\star$ (discussed in § 2.5). With the amount of gas lost to star formation and outflows at each timestep, the infall rate is also known at all timesteps. The results of all three are shown in Fig. 4.

2.5 Star Formation Efficiency

• The term "star formation efficiency" (SFE) is an overloaded term in the literature. In the star formation/feedback literature, it usually refers to the fraction of a molecular cloud's mass which will eventually be converted into stars. In the chemical evolution literature, however, it usually refers to the inverse timescale relating the star formation rate within some gas reservoir and the mass of the gas reservoir itself: $\tau_\star \equiv \Sigma_{\rm g}/\dot{\Sigma}_\star$. High (Low) values of $\tau_\star$ indicate slow (fast) star formation and thus low (high) SFE; when we refer to SFE here, we're referring to the definition based on this timescale. In the star formation literature, this parameter is often referred to as the "depletion time."

• Based on the findings of Kennicutt (1998), it is common practice for chemical evolution studies to implement a single power-law star formation law of the form:

$$\dot{\Sigma}_\star \sim \Sigma_{\rm g}^N \tag{13}$$

where $\dot{\Sigma}_\star$ and $\Sigma_{\rm g}$ are the surface densities of star formation and ISM gas, respectively, and Kennicutt (1998) derive $N = 1.4 \pm 0.15$ relating the total $\dot{\Sigma}_\star$ and $\Sigma_{\rm g}$ within the disc across a sample of quiescent spiral galaxies and infrared and circumnuclear starbursts. However, recent studies have found evidence that much of the observed scatter is physical in origin (de los Reyes & Kennicutt 2019) and that there are significant breaks in both the power-law index and zero-points (Kennicutt & de los Reyes 2020). Much of the uncertainty surrounding the details of the star formation law is a consequence of the ongoing debate about the CO-to-H_2 conversion factor (Kennicutt & Evans 2012; Liu et al. 2015). Although Ellison et al. (2020a) demonstrate that there are significant galaxy-to-galaxy variations in the star formation law, suggesting that individual galaxies do not follow the population-averaged trend, de los Reyes & Kennicutt (2019) argue that this is still a reasonable recipe for Galaxy evolution models. We adopt such a formalism here.

• Krumholz et al. (2018) compare model-predicted star formation laws to the observational data from Bigiel et al. (2010) and Leroy et al. (2013) (see their Fig. 2). We find that the following by-eye fit to the power-law index N is a reasonable description of the aggregate data:

$$N = \begin{cases} 1.0 & (\Sigma_{\rm g} \geq \Sigma_{\rm g,2}) \\ 3.6 & (\Sigma_{\rm g,1} \leq \Sigma_{\rm g} \leq \Sigma_{\rm g,2}) \\ 1.7 & (\Sigma_{\rm g} \leq \Sigma_{\rm g,1}) \end{cases} \tag{14}$$

where $\Sigma_{\rm g,1} = 5 \times 10^6$ M$_\odot$ kpc^{-2} and $\Sigma_{\rm g,2} = 2 \times 10^7$ M$_\odot$ kpc^{-2}.

• The apparent linearity of the relationship above $\sim 2 \times 10^7$ M$_\odot$ kpc^{-2} suggests that in this regime, star formation is proceeding at the fastest possible rate, and that $\tau_\star = \Sigma_{\rm g}/\dot{\Sigma}_\star$ = constant. The results of Leroy et al. (2008, 2013) and Kennicutt & de los Reyes (2020) would suggest that this is the regime in which the molecular fraction $f_{\rm mol} = M_{\rm H_2}/(M_{\rm HI} + M_{\rm H_2}) \approx 1$. We therefore adopt the assumption that above $\Sigma_{\rm g} = 2 \times 10^7$ M$_\odot$ kpc^{-2}, $\tau_\star$ reaches its minimum value, and increases with decreasing $f_{\rm mol}$. We denote this value as $\tau_{\rm mol}$, the value of $\tau_\star$ for a gas reservoir with $f_{\rm mol} = 1$. This, combined with our three-component power-law index N results in the following final form for our adopted star formation law:

$$\dot{\Sigma}_\star = \begin{cases} \Sigma_{\rm g}\tau_{\rm mol}^{-1} & (\Sigma_{\rm g} \geq \Sigma_{\rm g,2}) \\ \Sigma_{\rm g}\tau_{\rm mol}^{-1}\left(\frac{\Sigma_{\rm g}}{\Sigma_{\rm g,2}}\right)^{2.6} & (\Sigma_{\rm g,1} \leq \Sigma_{\rm g} \leq \Sigma_{\rm g,2}) \\ \Sigma_{\rm g}\tau_{\rm mol}^{-1}\left(\frac{\Sigma_{\rm g,1}}{\Sigma_{\rm g,2}}\right)^{2.6}\left(\frac{\Sigma_{\rm g}}{\Sigma_{\rm g,1}}\right)^{0.7} & (\Sigma_{\rm g} \leq \Sigma_{\rm g,1}) \end{cases} \tag{15}$$

where we chose the power-law indeces such that this formalism is consistent with equation (14), and prefactors are added to ensure piece-wise continuity. In implementation, `VICE` requires the $\tau_\star - \Sigma_{\rm g}$ relationship when ran in infall and gas modes, and the $\tau_\star - \dot{\Sigma}_\star$ relationship when ran in star formation mode. Both follow from this relationship given the substitution $\tau_\star \equiv \Sigma_{\rm g}/\dot{\Sigma}_\star$.

– Although it is more physically motivated to use an adopted star formation law to infer a star formation rate from the ISM properties at a given timestep, as discussed in § 2.4, we are using `VICE` in star formation mode, meaning that it is $\dot{\Sigma}_\star$ rather than $\Sigma_{\rm g}$ or $\dot{\Sigma}_{\rm in}$ which is specified *a priori*. Therefore, our models are inferring $\Sigma_{\rm g}$ from $\dot{\Sigma}_\star$, not the other way around.

• Based on the observed Kennicutt-Schmidt relation at different redshifts, Tacconi et al. (2018) suggest that $\tau_{\rm mol}$ should scale with redshift z and the deviation from the star forming main sequence δMS via $\tau_{\rm mol} \propto (1+z)^{-0.6}\delta{\rm MS}^{-0.44}$. We don't take into account the effect of δMS in our models, but we do investigate the redshift dependence. A reasonable approximation to the $t - z$ relation out to $z \approx 3$ assuming typical ΛCDM cosmology is given by:

$$\frac{t}{t_0} \approx (1+z)^{-5/4} \tag{16}$$

where t_0 is the present-day age of the universe, and t is not simulation

time but the age of the universe at any given redshift. Plugging this relation into the Tacconi et al. (2018) scaling yields the following time-dependence for $\tau_{\rm mol}$:

$$\tau_{\rm mol} = \tau_{\rm mol,0}(t/t_0)^{12/25} \approx \tau_{\rm mol,0}(t/t_0)^{1/2} \quad (17)$$

where $\tau_{\rm mol,0}$ is simply $\tau_{\rm mol}$ at the present day. We generalize this formula to the following form:

$$\tau_{\rm mol} = \tau_{\rm mol,0}(t/t_0)^{\gamma} \quad (18)$$

In this paper we present simulations which adopt $\tau_{\rm mol,0}$ = 2 Gyr (Leroy et al. 2008, 2013; Tacconi et al. 2018) and γ = 1/2 based on this argument. We have also ran simulations which adopt $\tau_{\rm mol,0}$ = 1 Gyr and γ = 0 (a time-independent $\tau_{\rm mol}$), and found similar results.

- At all timesteps in our models, $\Sigma_{\rm g}$ is inferred from $\dot{\Sigma}_\star$ directly from equations (15) and (18). The infall rate is subsequently calculated from the amount of gas lost to new stars and outflows within a given timestep and the amount of gas implied by the star formation rate at the next timestep, and is assumed to be zero metallicity.
- Fig. 5 shows $\tau_\star$ as a function of $R_{\rm gal}$ at six different time stamps predicted by our fiducial, inside-out SFH model. At $R_{\rm gal} \lesssim 6$ kpc, $\tau_\star$ is near $\tau_{\rm mol}$ at all times, implying a molecular fraction of unity at these radii. Although this prediction is likely unrealistic (citation?), relaxing our assumptions about the star formation law does not significantly impact our conclusions. In collecting results for this paper, we investigated purely linear, purely power-law, and broken power-law star formation laws, finding similar predictions in all cases. In practice we find that the detailed form the star formation history and, to some extent, the time-dependence of radial migration have much more power over the model predictions. We interpret this as an indication that the details of the star formation law are at most secondary effects in establishing the model behavior.

2.6 Surface Density Gradient

- As discussed in § 2.4, Appendix A presents justification of a recipe in which we select a unitless, unnormalized form describing the scaling of the stellar surface density with Galactocentric radius, denoted $g(R_{\rm gal})$. Here we adopt the following double exponential form, describing the thin and thick discs of the Milky Way:

$$g(R_{\rm gal}) = e^{-R/R_t} + \frac{\Sigma_T}{\Sigma_t} e^{-R/R_T} \quad (19)$$

where R_t and R_T are the scale radii of the thin and thick discs, respectively, and Σ_T/Σ_t is the ratio of their surface densities at $R_{\rm gal}$ = 0. In this paper, we adopt R_t = 2.5 kpc, R_T = 2.0 kpc, and Σ_T/Σ_t = 0.27 from the findings of Bland-Hawthorn & Gerhard (2016). These are illustrated by the two dotted black lines in Fig. 6, with the solid one denoting the sum of the two. Both have been re-normalized such that the integral over the surface area of the model Galaxy implies a total stellar mass in agreement with our adopted value.

- Adopt the Licquia & Newman (2015) total stellar mass of $(6.08 \pm 1.14) \times 10^{10}\ M_\odot$. We're including bulge star particles in our sample of candidate analogs from `h277`, so we model the entire stellar mass as opposed to just the disc, for which Licquia & Newman (2015) found $(5.17 \pm 1.11) \times 10^{10}\ M_\odot$. This choice only matters in setting the overall normalization of our adopted star formation histories $\dot{\Sigma}_\star$ as a function of radius and time, in turn affecting the inferred gas surface density $\Sigma_{\rm g}$ via our adopted star formation law (see discussion in § 2.5). In short, lower (higher) stellar masses suggest longer (shorter) values of $\tau_\star$ at all times. This only impacts our models insofar as our choice about the star formation law matters;

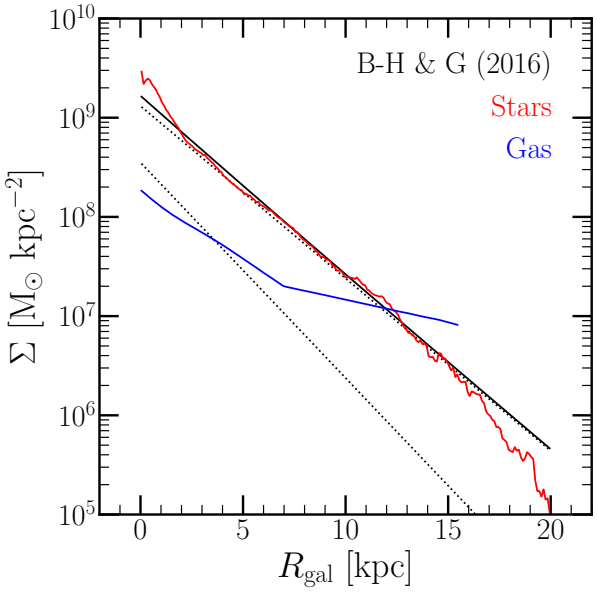

Figure 6. The surface density of gas (blue) and stars (red) as predicted by our inside-out SFH model. The dotted black line with the higher normalization denotes a thin disc profile with scale length R_t = 2.5 kpc; the other denotes a thick disc profile with scale length R_T = 2.0 kpc, and a ratio of Σ_T/Σ_t = 0.27 at $R_{\rm gal}$ = 0. The solid black line denotes the sum of the two; this is the surface density gradient of the Milky Way as reported by Bland-Hawthorn & Gerhard (2016), renormalized to imply the same total stellar mass within the disc.

as discussed in § 2.5, we find in practice that varying those assumptions don't impact our conclusions. We find the same for models with a different present-day stellar mass.

- Surface density gradient from fiducial model with inside-out SFH, plotted in Fig. 6 (stars in red and gas in blue). Radial migration indeed didn't change the overall scaling of $\Sigma_\star$ with $R_{\rm gal}$ at the radii that we care about in this paper (3 kpc $\lesssim R_{\rm gal} \lesssim$ 15 kpc), only introducing scatter. Gas disc appears to flatten at $R_{\rm gal} \gtrsim 6$ kpc; this is a consequence of our model for star formation efficiency (see discussion in § 2.5). The radius at which $\Sigma_{\rm g}$ shows a break in Fig. 6 coincides with the radius at which $\Sigma_{\rm g}$ is low enough to transition from the $\dot{\Sigma}_\star \sim \Sigma_{\rm g}$ to the $\dot{\Sigma}_\star \sim \Sigma_{\rm g}^{3.6}$ piece of our adopted star formation law. With our star formation histories specified *a priori*, these choices impact the radial profile of $\Sigma_{\rm g}$.

2.7 Summary

- In summary, our fiducial model has an inside-out SFH (see §2.4) with the star formation law as described in §2.5, radial migration the proceeds according to the diffusion model (see § 2.2), and yields and outflows as described in § 2.3.
- We have also conducted runs with the three other SFHs, the three other migration prescriptions, and the three other SFE prescriptions - a total of 64 simulations, as well as a variety of other test cases. In this paper, we present results wherever the model predictions are sensitive to the assumptions. However, in general the differences can be understood with only the variations in star formation history and the qualitative notion that many stars have moved beyond their birth radius.
- To ensure that resolution does not affect our results, we ran

the same set of models with $n = 2$ stellar populations per zone per timestep, and found similar predictions.

3 COMPARISON TO OBSERVATIONS

• Fig. 7 shows a scatter plot of 10,000 randomly sampled stellar populations in five bins of $R_{\rm gal}$ and three bins of $|z|$ ($R_{\rm gal}$ = 3 - 5 kpc, 5 - 7 kpc, 7 - 9 kpc, 9 - 11 kpc, and 11 - 13 kpc; $|z|$ = 0 - 0.5 kpc, 0.5 - 1 kpc, and 1 - 2 kpc). These are the same bins and same scheme for organizing the panels as in Fig. 4 of Hayden et al. (2015).

• The width of the low-α sequence predicted by the model comes from radial migration. Though this wouldn't occur without radial migration, our models by construction predict an ISM which spends most of its time near the equilibrium abundance along the low-α sequence with a built-in metallicity gradient. For this reason, it's only natural that our models predict this to be the case, although nonetheless it is in good agreement with Schönrich & Binney (2009) and Nidever et al. (2014).

• The low-α sequence shifts from a high [Fe/H] locus at small $R_{\rm gal}$ to low [Fe/H] at high $R_{\rm gal}$, in agreement with the observed distributions in APOGEE presented in Hayden et al. (2015).

• High-α stars are most prevalent at low $R_{\rm gal}$ and high $|z|$, and conversely for the low-α stars, also in agreement with Hayden et al. (2015).

– Similar results are found for different SFHs. This suggests that this observed result is a natural consequence of stellar migration.

– Only minor difference worth noting is that the starburst models predict a slightly higher characteristic [O/Fe] (∼+0.1) for the low-α sequence. This is a natural consequence of the starburst producing young, α-enhanced stars (Johnson & Weinberg 2020).

3.1 Abundance Gradients

• Left-hand panel of Fig. 8 compares the tracks predicted by our fiducial, inside-out SFH assuming diffusion migration (solid lines) versus post-processing (dotted lines) for the gas-phase of a handful of radii denoted by the legend. Predicted [O/Fe]-[Fe/H] tracks for the diffusion model show significant deviations from the post-processing model. We demonstrate here that this is due to variability in the SN Ia rate induced by the time-dependent radial migration of the diffusion model. Simulation times of 2, 4, 6, 8, 10, and 12.2 Gyr shown in points and X's for the two models.

– For each zone, `VICE` provides in its outputs the rates of infall and star formation, the mass of the ISM, and the relevant abundance information for each element along with the associated MDFs at the final timestep. To determine the SN Ia rates, we therefore have to approximate from the output.

– From the `VICE` outputs of our models, we extract a proxy for the SN Ia rate by isolating the contribution from SNe Ia to the time derivative of the Fe mass. The total time derivative can be obtained by the difference in Fe mass across two timesteps; then subtracting the contribution from CCSNe and approximately correcting for recycling yields an estimate of $\dot{M}_{\rm Fe}^{\rm Ia}$.

– This proxy is plotted against simulation time in the right-hand panel of Fig. 8 for the same annuli as in the left-hand panel, with multiplicative factors added for visual clarity, diffusion model again shown in solid lines, post-processing in dotted lines. Whenever and wherever there is a deficit in SN Ia events relative to the post-processing model, the diffusion model tends toward higher [O/Fe] values than the post-processing scenario. Conversely, lower [O/Fe] for an excess in SN Ia events.

– SN Ia rates show high-amplitude variability on Gyr timescales, with low-amplitude white-noise on shorter timescales, potentially introduced at least in part by our discretization of the disc into annuli and the evolution into timesteps. The log-scaled y-axis makes it clear that the fractional amplitude is higher near the outskirts of the disc. This makes physical sense, because the stellar number density is much lower there, and as such would be much more susceptible to sampling noise - that is, a single star migrating has a larger fractional impact on the stellar density and thus the supernova rates at large radii than small radii.

– Fluctuations in the SN Ia rate at these amplitudes can be understood through a comparison of the timescales associated with orbital migration and SN Ia event delays. In the top panels of Fig. 1, we note that the distribution of $R_{\rm Final}$ is significantly more peaked in the 0 - 2 Gyr age bin than for older stars. Despite this, the value of the PDF in all radial bins implies ∼40-50% of `h277` star particles migrated significantly beyond their birth radius by the time they were 2 Gyr old. Though we adopt a different form in detail here, the SN Ia DTD is to order of magnitude a t^{-1} power-law with a minimum delay of ∼100 Myr (Maoz & Mannucci 2012; Maoz & Graur 2017). With this DTD, there are the same number of SN Ia events with delay-times between 100 Myr and 1 Gyr as between 1 Gyr and 10 Gyr. Combining these two pieces of information would suggest that a significant fraction of SN Ia progenitors migrate significantly beyond their birth radius. That is, while radial migration is often described as a slow process, so is the SN Ia DTD due to its long tail. With this realization, variability in the SN Ia rate at the levels seen in our models is not surprising.

• This is proof of concept that radial migration of nucleosynthetic yields can occur alongside stellar migration for delayed sources. In general, the characteristic delay-time for SN Ia events is ∼1 Gyr, and stellar migration is proceeding on similar timescales in our models. In principle, it is reasonable to expect similar effects for s-process elements like carbon, nitrogen, strontium, yttrium, zirconium, etc. which are produced in AGB stars and thus have similar characteristic delay-times, though we do not investigate the impact for these elements here.

• What we really learn from this investigation is that when stellar migration is taken into account, tracks are not simple functions. To first order, they are characterized by the late-time equilibrium abundance and the value of $\tau_\star$ setting the position of the "knee" (Weinberg et al. 2017), though migration causes noticeable variations,

• Demonstrate in § 3.4 that this is a means with which to form α-rich and α-poor stars - or rather Fe-poor and Fe-rich, respectively.

• The top row of Fig. 9 shows the radial [O/H] and [Fe/H] gradients, with the [O/Fe] gradient in the bottom row. In all panels, stars show the median abundance in each annulus, and the shaded regions denote the 16th and 84th percentiles of the MDF in that zone. Solid lines show the gas-phase gradient at the present day. Although we built the abundance gradient into our models based on the mode abundance at a given radius, we illustrate the gradients here according to the median. We find that with annuli as narrow as $\Delta R_{\rm gal}$ = 100 pc, the mode is a sufficiently noisy statistic to introduce noticeably more scatter in this relation. Nonetheless, we

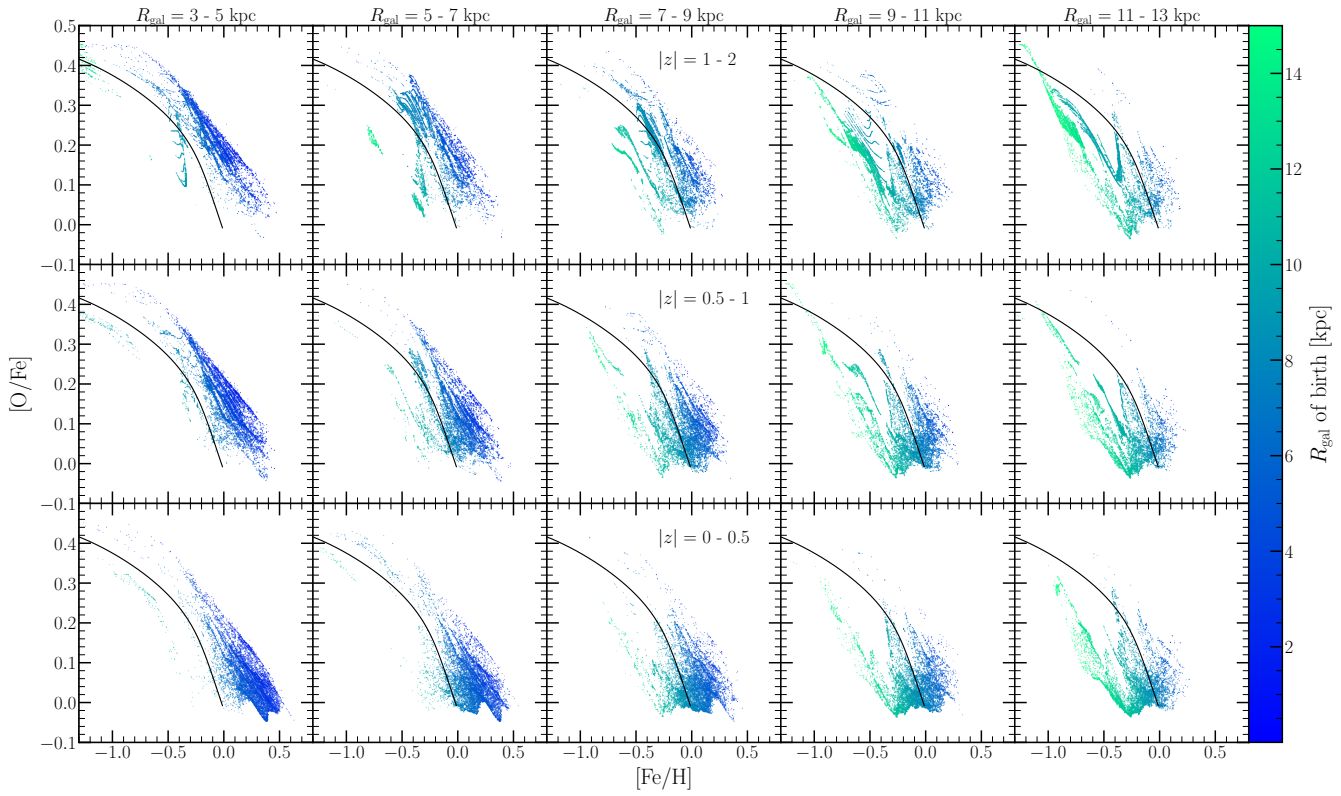

Figure 7. [O/Fe]-[Fe/H] diagrams for 15 galactic regions spanning five bins in R_{gal} and $|z|$. Each region has its own panel, with radial bins shown in columns denoted at the top of the figure, and with $|z|$ bins shown in rows denoted in text in the middle column. In each panel, we plot N = 10,000 points sampled from our simulated stellar populations in each region predicted by our inside-out SFH, where the probability of sampling is proportional to the present-day mass of each stellar population. In all panels points are color-coded according to the Galactocentric radius of birth of the stellar population. For reference, we plot in a solid black line in all panels the gas-phase [O/Fe]-[Fe/H] track predicted by the same SFH in the R_{gal} = 8 kpc annulus, but with the post-processing migration model; this curve is the same in all panels.

have verified that it follows the trend implied by our target gradient (see § 2.3), illustrated by the solid black line in the top panels. We note that the median gradient follows a slightly shallower trend that the mode, which is expected when the metallicity distribution is skew-negative in the inner Galaxy and skew-positive in the outer Galaxy.

- Gradient is indeed recovered in [O/H], and radial migration appears to only induce scatter. While Fe did not enter into our procedure for setting the metallicity gradient, the model predicts a similar gradient for [Fe/H].
- Clear that the MDF shows a metal-rich mode and skew-negative shape in the inner galaxy for both O and Fe. α-enhanced tail there as well. We demonstrate in § 3.1 that the MDF does shift to skew-positive in the outer galaxy, though this isn't as visually obvious from this plot due to the scatter in the mode at these radii. We investigate the MDFs at different radii in detail in § 3.2.
- All models predict the [O/Fe] gradient to be relatively flat throughout the disk, steepening only in the inner ~few kpc and beyond 15.5 kpc, where we shut off star formation. The trend in our predicted abundances toward higher [α/Fe] at large R_{gal} is expected for this reason; all stellar populations currently at R_{gal} > 15.5 kpc formed in the disc and migrated there. Only the stars old enough to migrate to such radii will be located there at the present day, and since these stars are old, they're also α-enhanced. This is consistent with the findings of Radburn-Smith et al. (2012), who argue that the outskirts of the NGC 7793 disc formed largely out of radial migration of stars.
- We note that there are differences between the stellar and gas-phase gradients in all models. We therefore argue that it'd be reasonable to expect differences in reported slopes and normalizations of the gradient in observational studies, particularly in the inner Galaxy.
- Stellar gradient is somewhat shallower in the late-burst model; this is because of the dilution associated with the starburst. Target gradient represents the equilibrium abundance at all radii, and we deliberately perturbed it from equilibrium, so any deviations from the expectation are a consequence of that.
- Late-burst model has super-equilibrium gas phase abundance at the present day. Can be seen by comparing it to the outer-burst model's gas phase gradient and seeing that it has a break at R_{gal} = 6 kpc, the threshold for the late starburst in this model. This is a consequence of the starburst as well - in infall driven starbursts, re-enrichment can produce super-equilibrium abundances which then decay back to the equilibrium abundance as the star formation rate declines (Johnson & Weinberg 2020).

3.2 Metallicity Distribution Functions

- MDFs in bins of Galactocentric radius are a fundamental observable to test the validity of any chemical evolution model. In this

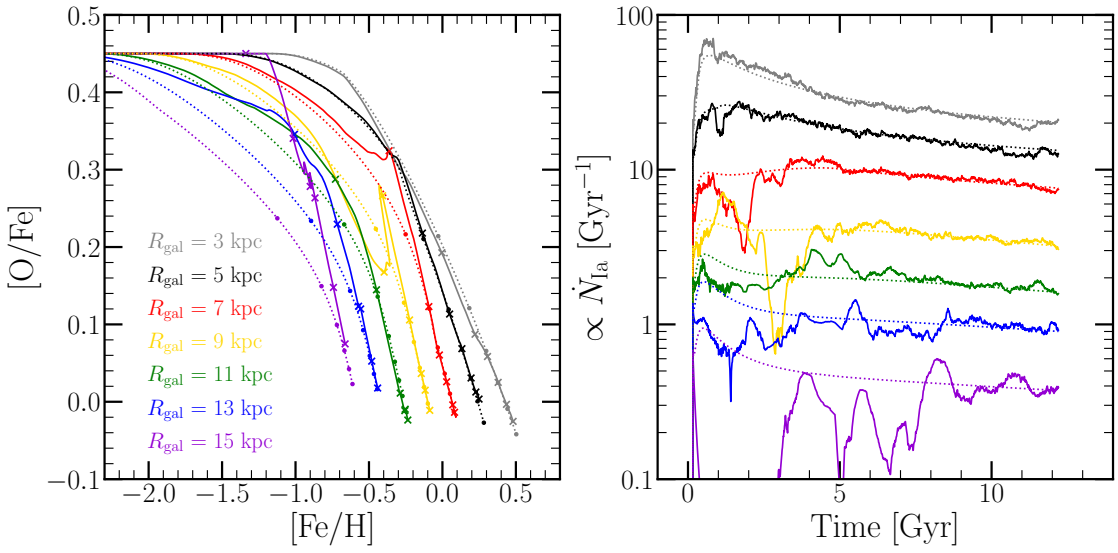

Figure 8. Left: Gas phase evolutionary tracks in the [O/Fe]-[Fe/H] plane for our inside-out SFH with either post-processing (dotted lines) or diffusion (solid lines) migration models. We plot tracks for seven annuli, color-coded according to their Galactocentric radius and denoted by the legend in the lower-left. We mark simulation times of 2, 4, 6, 8, 10, and 12.2 Gyr in X's for the diffusion model and points for the post-processing model. **Right**: As a function of simulation time, a proxy for the SN Ia rate using the total time-derivative of the Fe mass in a given annulus, calculated by subtracting the contribution from recycling and CCSN enrichment and adding back that lost to star formation and outflows. We show these rates for the same annuli as in the left-hand panel, multiplying them by various prefactors to improve clarity.

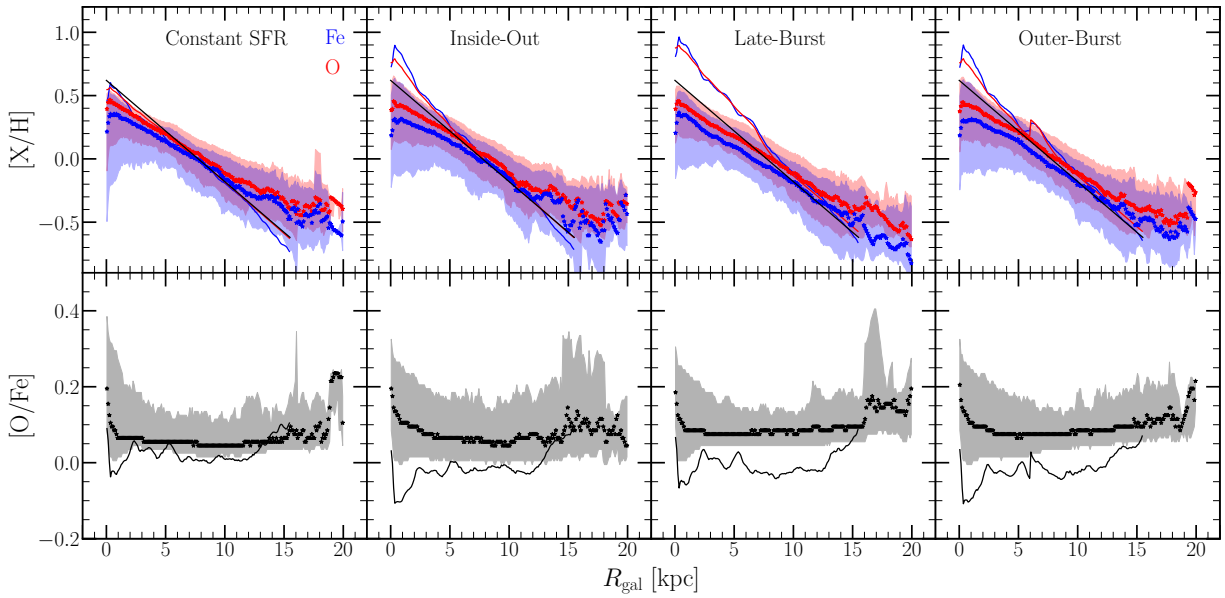

Figure 9. Radial abundance gradients in [O/H] (top, red) [Fe/H] (top, blue), and [O/Fe] (bottom) for our four fiducial SFHs - constant (far left), inside-out (left-middle), late-burst (right-middle), and outer-burst (far right). We plot the gas phase abundance at the present day as a function of Galactocentric radius in solid lines. Stars denote the median of the stellar MDF of the 100-pc width annulus at a given radius, with shaded regions marking the 16th and 84th percentiles thereof. Black lines in the top panels denote our target [α/H] gradient of mode([α/H]) = +0.3 at $R_{\rm gal}$ = 4 kpc with a slope of -0.08 kpc^{-1}.

section we compare our predicted MDFs to those observed in the 16th data release (DR16; Ahumada et al. 2020) of the Apache Point Observatory Galaxy Evolution Experiment (APOGEE; Majewski et al. 2017). The data is reduced using the APOGEE Stellar Parameters and Chemical Abundances Pipeline (ASPCAP; Holtzman et al. 2015; García Pérez et al. 2016). For further details on the APOGEE survey, a brief summary can be found in § 2 of Weinberg et al. (2019).

• We restrict our sample to stars with effective temperatures of 4000 K $\leq T_{\rm eff} \leq$ 4600 K, surface gravities of 1.0 $\leq \log g \leq$ 2.5, and signal-to-noise ratios of at least 100. These cuts ensure that our sample consists of stars on the upper red giant branch,

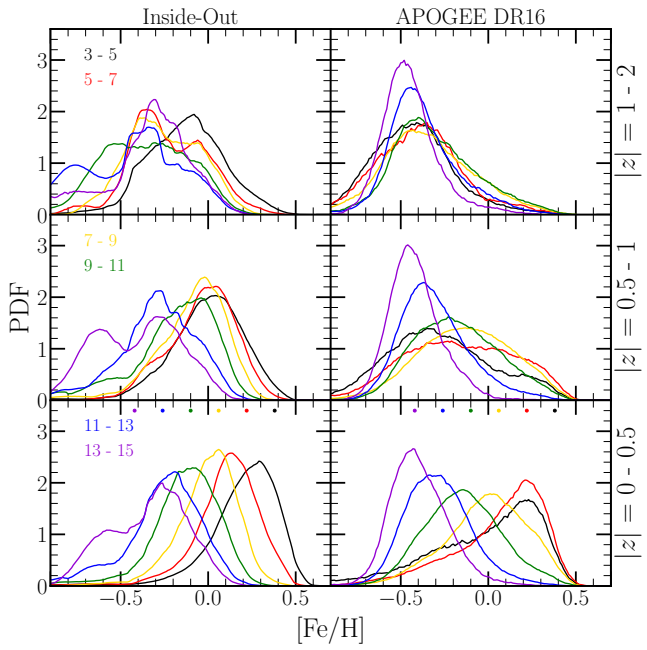

Figure 10. Metallicity Distribution Functions in [Fe/H] predicted by our fiducial model (left) and as observed in APOGEE DR16 (right), for stars and simulated stellar populations with present day $|z|$ = 0 - 0.5 kpc (bottom), 0.5 - 1 kpc (middle), and 1 - 2 kpc (top). MDFs are shown in bins of Galactocentric radius: 3 - 5 kpc (black), 5 - 7 kpc (red), 7 - 9 kpc (yellow), 9 - 11 kpc (green), 11 - 13 kpc (blue), and 13 - 15 kpc (purple). The points near the top of the bottom panels denote what the mode abundance would be if it followed our target gradient of [Fe/H] = +0.3 at $R_{\rm gal}$ = 4 kpc and a slope of -0.08 kpc^{-1}, assuming the inner radius of each bin (i.e. there is no point plotted for 15 kpc). All distributions are smoothed with a box-car width of [Fe/H] ± 0.1.

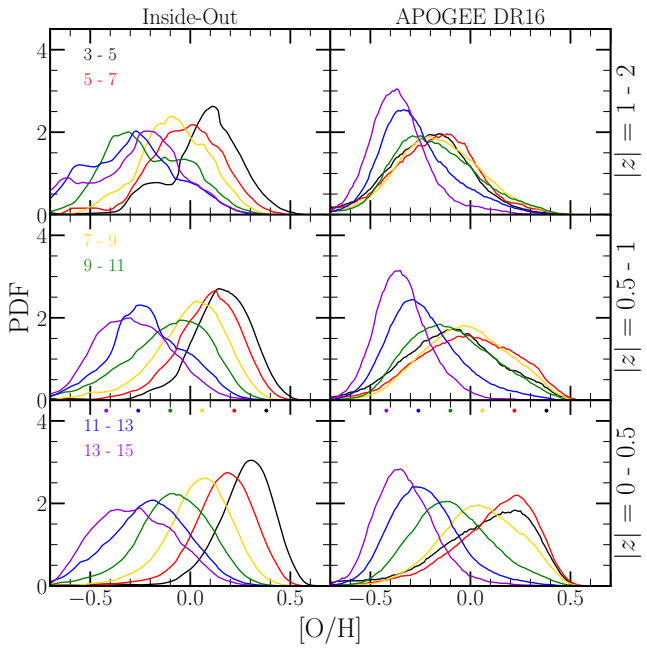

Figure 11. The same as Fig. 10, but for [O/H].

safely excluding red clump stars to avoid obvious systematics in the abundance distributions.

• Previously known that the MDFs in the disc midplane as observed in APOGEE show mode [α/H] and [Fe/H] abundances that depend on Galactocentric radius, with a skew-negative distribution in the inner Galaxy and a skew-positive distribution in the outer Galaxy. Off the midplane, the MDFs merge and converge on [α/H] ≈ [Fe/H] ≈ -0.5 (Hayden et al. 2015; Weinberg et al. 2019). This result is replicated for the observations in the right-hand column of panels in Fig. 10 and Fig. 11.

– Similar mode [O/H] and [Fe/H] between the 3 - 5 and 5 - 7 kpc in the APOGEE observations. What could be the origin of this? One possibility is that our formalism for $\eta(R_{\rm gal})$ is incorrect. We would expect a both a flat [X/H] gradient and MDFs with similar modes if we simply chose it to be so by letting η be constant in the inner galaxy. Another possibility is the cessation of star formation in the inner Galaxy (see Fig. 1 of Peek 2009 and Fig. 2 of Fraternali & Tomassetti 2012), an effect which also isn't included in our models. If the Milky Way has begun quenching, a process believed to begin in the centres of galaxies at this mass (e.g. Ellison et al. 2020b), then few stars would form in the most metal-rich regions, cutting off the MDF at high [O/H] and [Fe/H].

• Left-hand panels of Figs. 10 and 11 show the distributions predicted by our late-burst model. They successfully replicate the qualitative result that the mode [X/H] varies with present-day Galactocentric radius, but fail to show a similar mode abundance between the 3 - 5 and 5 - 7 kpc bins. Potentially linked to the cessation of star formation in inner Galaxy (Peek 2009; Fraternali & Tomassetti 2012), not included in our models.

• Beyond the midplane, our models fail to fully replicate the convergence of the MDFs at [X/H] ≈ -0.5. The observed MDF at small radii shifts from skew-negative with a metal-rich mode to skew-positive with a metal-poor mode with increasing $|z|$. In our predicted MDFs for the inner galaxy, the mode does shift to lower [X/H], though not to the same extent as in the observations. There is also very little change in skewness with $|z|$ predicted, in tension with observations.

• We note that our models do a good job of producing a mode [X/H] abundance in each radial bin close to our target gradient (shown as points plotted at the top of the bottom panels in Fig. 10 and 11 for the inner radius of each 2 kpc bin). In the inner galaxy bins, the predicted mode is moderately lower than the target, but this is due to the effect of dilution (see discussion in § 3.5). In our inside-out and outer-burst models, the difference in target and predicted mode [X/H] is considerably smaller.

3.3 [O/Fe] Distributions in Bins of [Fe/H]

• In this section we compare our model predicted [O/Fe] distributions to those published in Vincenzo et al. (2021). These are intended to simultaneously remove the effects of observational errors in [O/Fe] and the APOGEE selection function in these Galactic regions; that is, these are estimates of the *intrinsic* [O/Fe] distributions that, when convolved with observational uncertainties and the APOGEE selection function, would resemble the observed MDFs.

• Fig. 12 show distributions in [O/Fe] in two bins of [Fe/H] across 15 Galactic regions predicted by our inside-out SFH (solid lines). Dashed lines show the Vincenzo et al. (2021) distributions.

• We note that our model adequately reproduces the broad nature

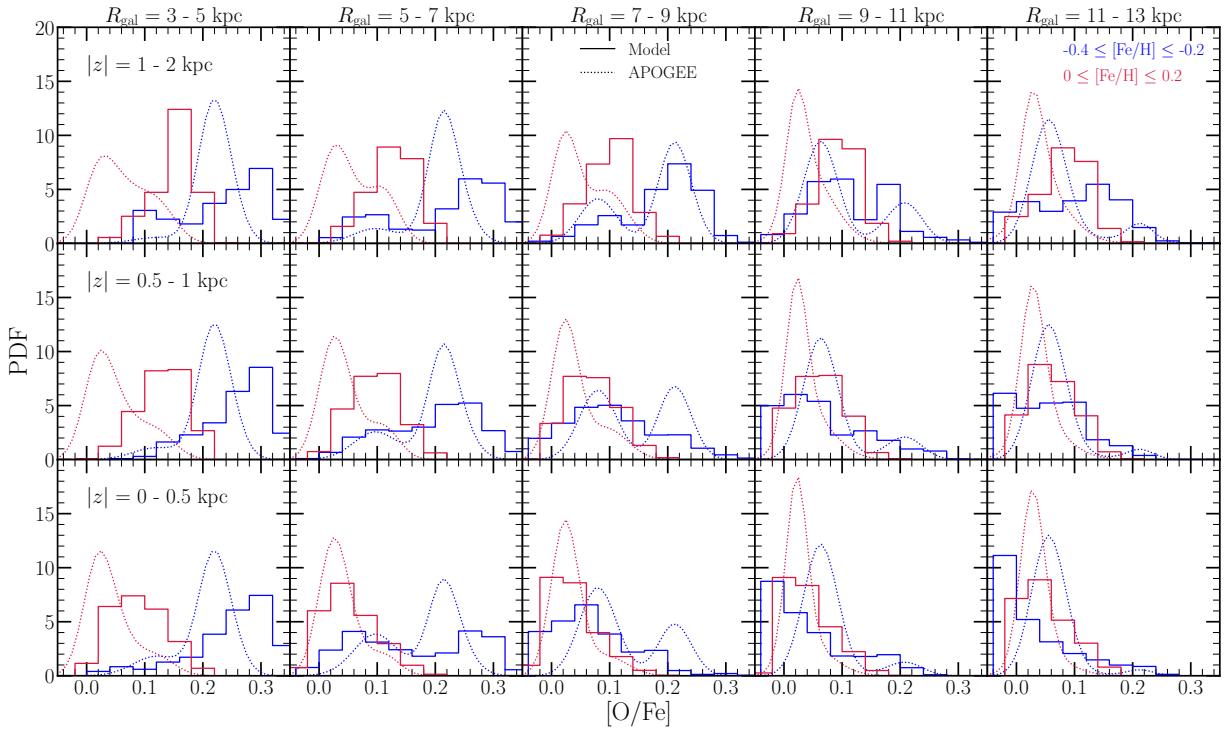

Figure 12. Predicted distributions in [O/Fe] in 15 Galactic regions and in two bins in [Fe/H]. Columns correspond to bins in R_{gal}, denoted at the top of each column. Rows correspond to bins in $|z|$, denoted in text in the left-hand column. Distributions are color-coded according to the [Fe/H] the sample is drawn from, denoted by the legend in the upper right panel. Solid lines represent that predicted by our inside-out SFH in Δ[O/Fe] = 0.04 bins, while dashed lines correspond the fits to the APOGEE DR16 data presented in Vincenzo et al. (2021), which quantify the intrinsic distributions accounting for observational uncertainties and the APOGEE selection function.

of the [O/Fe] distributions at fixed [Fe/H] seen in the APOGEE data. A number of distributions show a bimodality in decent agreement with the observations (e.g. the -0.4 ≤ [Fe/H] ≤ -0.2 bin at R_{gal} = 3 - 5 kpc and $|z|$ ≤ 0.5 kpc), but this is not true of all Galactic regions in both metallicity bins. Instead, the the principle failure of a number of these distributions is that they overpredict the number of intermediate [O/Fe] stars. While our model is successful in some ways with regards to reproducing these distributions, it fails to describe the observations in detail in this way.

- In the inner galaxy, we overestimate the [O/Fe] of the highest [Fe/H] stars at all $|z|$, and the differences in the distributions gets smaller with increasing R_{gal}. The lower [Fe/H] bins don't seem to have this problem.

  – At fixed R_{gal} and [Fe/H], the Vincenzo et al. (2021, in prep) MDFs show two peaks in the distribution which do not change with $|z|$; only their relative heights vary. This is an assumption built into the model, but the agreement with the APOGEE data is good. At small R_{gal}, the observed distributions may shift slightly to higher [Mg/Fe], but only at the $\lesssim$0.05 level between $|z|$ ≤ 0.5 and 1 ≤ $|z|$ ≤ 2.0 (see their Fig. X). In contrast, our model predicted distributions show an increase in the mode [O/Fe] of ∼ 0.1 over the same dynamic range in $|z|$. This suggests that our model overpredicts the increase of [O/Fe] with increasing $|z|$ compared to the APOGEE distributions.

  – Small R_{gal} and high $|z|$ is a Galactic region where the APOGEE data are few, and the stellar number density is high, so it's possible the observations aren't well characterized. Indeed, in the R_{gal} = 3 - 5 and 5 - 7 kpc bins at $|z|$ = 1 - 2 kpc, the Vincenzo et al. (2021) model is fit to 31 and 17 stars, respectively. In comparison, there are 109 in the solar annulus, and all other bins have >75 stars in the fit.

  – If this discrepancy persists in subsequent APOGEE data releases, it's possible the origin is tied to the Sagittarius dwarf. The `h277` simulation had a major merger at a lookback time of ∼10 Gyr, and another close to the present day (verify this, and provide citation), different timing than the pericentric passages of the Sagittarius dwarf (Ruiz-Lara et al. 2020). More pericentric passages of a massive satellite could kinematically heat low-[α/Fe] disc stars to higher $|z|_{max}$ orbits, shifting these distributions to lower [O/Fe]. This is another instance where running these models with a different hydro-sim's star particles could be enlightening.

  – Another possibility: details of the dynamical history? Could bar evolution have something to do with it? Again, a different dynamical history via another hydro-sim would be enlightening.

- Similar results are found for our other SFHs.
- While the notion that an [α/Fe] dichotomy can arise out of radial migration alone was put forth in Schönrich & Binney (2009), and later explored by Nidever et al. (2014), this suggests that an inside-out star formation history combined with stellar migration is not conducive to predicting this observed result. The principle failure of this model is that it overpredicts the abundance of intermediate [α/Fe] stars. This could point to a handful of things.

  – If the bimodality is to arise out of inside-out Galaxy evolution and radial migration alone, the transition between low- and high-α sequences needs to occur faster than it does in these models. The analytic models of Weinberg et al. (2017) suggest that the approach to chemical equilibrium occurs on the order of the SFE

timescale $\tau_\star$. Although we've adopted a star formation law which is motivated by observational results (see discussion in §2.5), the failure of these models to reproduce the observed results suggests that inside-out Galaxy growth with such a star formation law is not conducive to forming the infamous dichotomy.

– Under our current assumptions, the simplest way to achieve this is to simply shut off star formation during the intermediate [α/Fe] phase in the simulations. This is indicative that two-infall evolutionary histories (e.g. Chiappini et al. 1997, 2001; Romano et al. 2010; Grisoni et al. 2017; Noguchi 2018; Spitoni et al. 2016, 2018, 2019, 2020, 2021) would improve the agreement between our model predictions and the observed distributions.

3.4 The Age-[α/Fe] Relation

• In this section, we compare our model predictions to the observational results of Feuillet et al. (2019). While we made use of APOGEE DR16 data in comparing our model predictions to the observed MDFs (Ahumada et al. 2020; Majewski et al. 2017), they make use of DR14 stars which have Gaia parallax measurements available (Abolfathi et al. 2018; Gaia Collaboration et al. 2018, for details on the APOGEE survey, see discussion in § 3.2). With their spatial and quality cuts, the final sample consisted of 77,562 stars.

• Feuillet et al. (2019) ages are measured via isochrone matching. Potentially give a little more detail, but that may be adequate for our purposes.

• In bins of [O/Fe], they assume a gaussian log-age distribution, and fit the mean and standard deviation to the observed sample. Because they assume a gaussian, they would report an equal mean and median. This is an important caveat in comparing our predicted relations to their results, because our model-predicted age distributions in bins of abundace are highly non-gaussian.

• The stellar populations from our simulations have different masses, so the age-distributions must be weighted by mass, since that scales with the number of stars that each stellar population represents. We therefore adopt a mass-weighted median age in bins of abundance as the appropriate comparison to the Feuillet et al. (2019) data. Physically, in a given bin [O/Fe], this is the age corresponding to the 50th percentile of the mass-weighted age distribution of our simulated stellar populations. For these reasons the comparison between our simulations and Feuillet et al. (2019) isn't exactly one-to-one. Potentially worth mentioning some of the systematics in calculating ages here as well, as that's relevant information.

• Fig. 13 shows a comparison between the predicted age-[α/Fe] relations in the solar annulus for our four migration models assuming our inside-out SFH.

• All models show reasonable agreement with the Feuillet et al. (2019) data; the population-averaged trend appears insensitive to the assumed migration model.

• Diffusion predicts the most intrinsic scatter, followed by linear, then sudden, then post-processing. This is a consequence of the variations in the SN Ia rates induced by time-dependent migration (see discussion in § 3). Further demonstration that under certain migration models, the radial migration of nucleosynthetic yields is statistically significant. This is also proof of concept that the effect is significant for abundance ratios of elements where at least one is produced by delayed nucleosynthetic sources. We therefore conclude that the time-dependence of radial migration is a necessary ingredient to chemical evolution models of galaxies where migration plays an important role, such as our own Milky Way. The level of scatter also appears to depend noticeably on which model for the time-dependence is adopted.

• This mechanism can produce populations of Fe-poor or Fe-rich stars, which can be misinterpreted as α-enhanced or α-deficient stars. Due to young stars migrating into or out of a given annulus, the SN Ia rate may be higher or lower than the expectation from a post-processing migration model. If this difference in the SN Ia rate is sustained for of order one depletion time, the ISM will be either Fe-poor or Fe-rich, and the stars that form there will inherit that composition. The stars that form out of that patch of ISM can then migrate to the solar annulus. This effect is most significant at large Galactocentric radii where the fractional amplitude of the variability in the SN Ia rate is largest, and for that reason the young Fe-poor population predicted by our diffusion model originates at large radii ($\gtrsim$ 12 kpc).

• Silva Aguirre et al. (2018) demonstrated that the observed young α-rich stars in the solar annulus have kinematics similar to the rest of the high-α population, and suggested that this may be the result of stellar mergers or mass transfer events, producing a population of truly old stars masquerading as young stars. In a sample of 51 of these stars on the red giant branch, Hekker & Johnson (2019) demonstrate that a portion of these stars have carbon-to-nitrogen ratios consistent with mass transfer events, but that others do not, indicating that either they're truly young stars or the results of mergers on the main sequence. Our model's prediction of intrinsically young, high [O/Fe] stars is independent of this mass transfer scenario; `VICE` does not include any statistical treatment of mass transfer events. Ascertaining the origins of this population therefore has implications for which of the migration models investigated here is the most realistic.

• Fig. 13 shows a comparison between the predicted age-[α/Fe] relations in the solar annulus for our four SFHs assuming diffusion migration.

• Constant and inside-out SFHs describe the observed data the best. Both late starburst models show a population-averaged increase in [α/Fe] at young ages which is not observed in the data. This challenges the results of Isern (2019) and Mor et al. (2019), suggesting that these results on the Milky Way recent SFH are not consistent with chemical evolution models. If the Milky Way truly experienced a recent starburst, something not included in our models had to occur to prevent this global increase in [α/Fe].

• Below [O/Fe] $\approx$ +0.1, the Feuillet et al. (2019) data seem to follow a slightly steeper age-[α/Fe] than our inside-out model predicts. This could point to inaccuracies in the detailed form of the SFH or the SN Ia DTD, our supernova yields, or observational [O/Fe] errors, all of which are very plausible.

• Fig. 14 presents a comparison of our simulation data to the Feuillet et al. (2019) observational data in 12 Galactic regions assuming the inside-out SFH.

• In the disc, the inside-out SFH is a reasonable description of the data for ages $\lesssim$ 5 Gyr, above which the median ages are overpredicted relative to Feuillet et al. (2019). Far from the midplane, our model overpredicts the ages at nearly all abundances where Feuillet et al. (2019) have data, with the exception of the $R_{\rm gal}$ = 7 - 9 kpc and $|z|$ = 0.5 - 1 kpc region.

• Feuillet et al. (2019) report ages for α-rich stars that are younger at large $R_{\rm gal}$ and high $|z|$, though in most cases only by ~20%. Our model, however, does not capture this effect. To illustrate this, we connect the black squares in the panel corresponding to the solar annulus with a solid black line, and reproduce this line in all panels as a reference. If the observational result is correct, this is an interesting result that our model doesn't reproduce in any of the variants we have examined.

• We note that the intrinsic scatter in the age-[α/Fe] relation

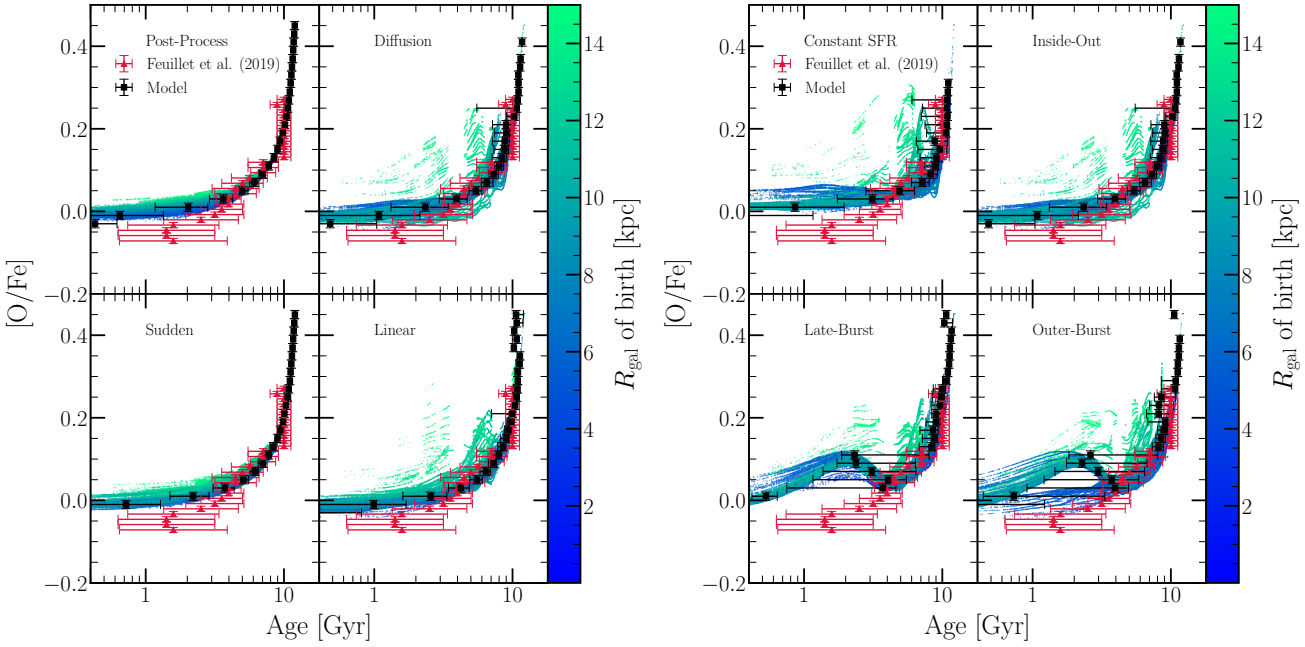

Figure 13. Left: A comparison of the predicted age-[O/Fe] relation for the solar annulus (R_{gal} = 7 - 9 kpc and $|z| \leq 0.5$ kpc) between the post-processing (upper left), diffusion (upper right), sudden (lower left), and linear (lower right) migration models, assuming our inside-out SFH. **Right**: The same as the left-hand panels, instead comparing the impact of our constant (upper left), inside-out (upper right), late-burst (lower left), and outer-burst (lower-right) SFHs, assuming diffusion migration. In all panels, red triangles and error bars denote the observed mean age and dispersion thereof in bins of [O/Fe] as reported by Feuillet et al. (2019); here we include only the bins containing at least 15 stars. Black squares denote the mass-weighted median age in 0.02-dex bins in [O/Fe] predicted by the simulations, with error bras denoting the 16th and 84th percentiles of the mass-weighted age distribution in those bins. Points in the background denote each individual stellar population from the simulation with a final position in the solar annulus, color-coded according to their Galactocentric radius of birth.

predicted by the model grows with increasing R_{gal}. Not only is the scatter in the colored background points visibly larger, but the error bars on the black points are as well, indicating that the age distribution is getting statistically significantly wider at fixed [α/Fe] with increasing R_{gal}.

– We identify two sources driving the increase in scatter at large R_{gal}. The bulk of the scatter, at least at [O/Fe] $\gtrsim +0.05$, arises from the variability in SN Ia rates as described in § 3.1. There, we demonstrated that the highest amplitude variability in the SN Ia rate in our model Galaxy occurs in the outskirts of the disc where the stellar number density is low. With higher variability in the SN Ia rate comes a higher variability in the gas-phase [O/Fe] ratio, resulting in an in-situ population whose age-[O/Fe] relation shows more intrinsic scatter compared to that at small radii. The second source is the change in normalization of the age-[O/Fe] relation expected for different star formation timescales. With decreasing τ_{sfh}, the age-[O/Fe] relation becomes shallower due to the delayed SN Ia enrichment channel depositing Fe into a depleted gas reservoir (Weinberg et al. 2017). This, coupled with the fact that the relation is intrinsically shallow at young ages, produces noticeable scatter near solar [O/Fe]. The comparison between the post-processing and diffusion migration models in Fig. 13 makes this fairly clear.

3.5 The Age-Metallicity Relation

• Although the age-metallicity relation (AMR) is usually formulated in age-[Fe/H], it is also interesting to look at age-[O/H] because it is not affected by SN Ia enrichment. The extent to which they differ indicates the extent to which the delayed timescale and impact of migration on SN Ia enrichment is important in shaping the age-[Fe/H] relation. Fig. 15 presents the age-[O/H] relation predicted by our constant-SFH model for the $|z| \leq 0.5$ kpc population at R_{gal} = 5 - 7, 7 - 9, 9 - 11, and 11 - 13 kpc. The black points quantify the same mass-weighted median age in bins of [O/H] as in §3.4. Colored points in the background are also the same - individual stellar populations color-coded according to birth radius. We choose the constant SFH model here because it is not subject to the effect of a time-varying SFH, as our fiducial inside-out SFH model is.

• The intrinsic scatter in the observed AMR has been interpreted as evidence for radial mixing for some time (e.g. Edvardsson et al. 1993). Feuillet et al. (2018) found that most of the metal-rich stars in the solar neighborhood were older than solar metallicity stars. Using the Weinberg et al. (2017) analytic models of one-zone chemical evolution, they argue that this is the result of old stars born at small R_{gal} where the equilibrium abundance is high migrating to the solar neighborhood. The fact that only the old stars are seen in the solar annulus can then be explained by the slow nature of radial migration.

• Fig. 15 extends our understanding of this effect. In all regions plotted, the intrinsic scatter in the bulk age-[O/H] relation increases noticeably with increasing age, and the color-coding of the background points makes it clear that this arises out of radial migration. At any given radius, the youngest stars form with a composition reflective of the local ISM, which in our models, is in turn reflective of the late-time equilibrium abundance at that radius. Stars with significantly different compositions were born in different Galactic regions and underwent radial migration.

– An interesting implication of this effect arises in the outer

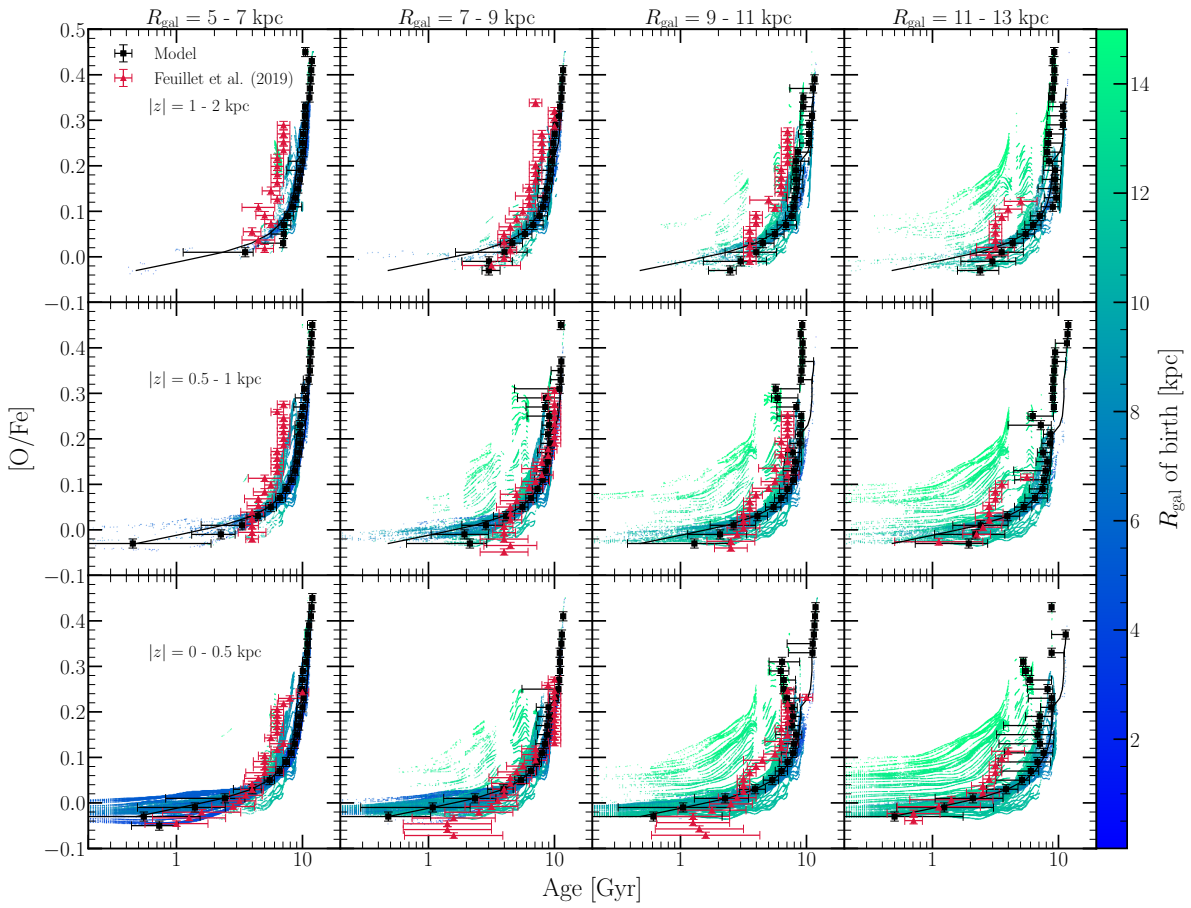

Figure 14. The age-[O/Fe] relation in 12 galactic regions predicted by our inside-out SFH. Bins in Galactocentric radius are shown in columns, and labeled at the top. Bins in the height $|z|$ above/below the disc midplane are shown in rows, noted in the left-hand column. Red triangles, black squares, error bars, and background points are as in Fig. 13 for the corresponding Galactic region. The solid black line connects the black squares in the bottom, left-middle panel, and is replicated in elsewhere for reference.

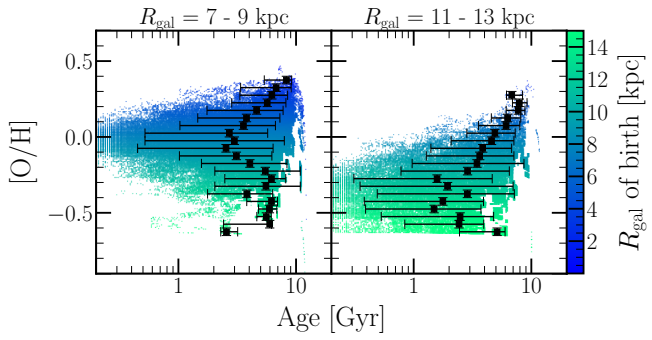

Figure 15. The age-[O/H] relation predicted by our constant SFR model for R_{gal} = 7 - 9 kpc (left) and 11 - 13 kpc (right). Each panel plots only the $|z|$ ≤0.5 kpc population. The colored points in the background and the black squares with error bars are as in Fig. 13, but with our binned, simulation prediction quantified in 0.05-dex bins in [O/H].

Galaxy, visible in the R_{gal} = 11 - 13 kpc bin. There, the equilibrium abundance is low, and the model predicts that nearly all other regions of the Galaxy are forming stars at higher abundances. When migration is taken into account, the result is an AMR which is nearly monotonically *increasing* with age, entirely the opposite of what is predicted by one-zone models.

- Furthermore, the characteristic metallicity of the youngest stars in a given radial bin decreases with increasing radius. This is a natural consequence of the abundance gradient that we've built in at late times, but interestingly, the effect is strong enough that at large radii, the median trend is nearly monotonically increasing with age. This is completely backwards from what is expected from one-zone models of chemical evolution for any radius. Since this is our constant-SFR model, it is not subject to the effects of a time-varying SFH, quantifying only what is caused by radial migration.
- Similar things are found for Fe, but the variations in the black squares a bit bigger so we demonstrate the effect with [O/H].
- Fig. 16 shows the age-[O/H] (top panel) and the age-[Fe/H] (bottom panel) relations predicted by our fiducial inside-out SFH in the solar annulus (R_{gal} = 7 - 9 kpc and $|z| \leq 0.5$ kpc), under the same plotting convention as in § 3.4. We add a solid black line to denote the Feuillet et al. (2018) AMR in comparison to that of Feuillet et al. (2019).

  – We note that we find similar results with regard to the age-[O/H] relation predicted by our models.
  – Feuillet et al. (2018) shows a significantly younger median

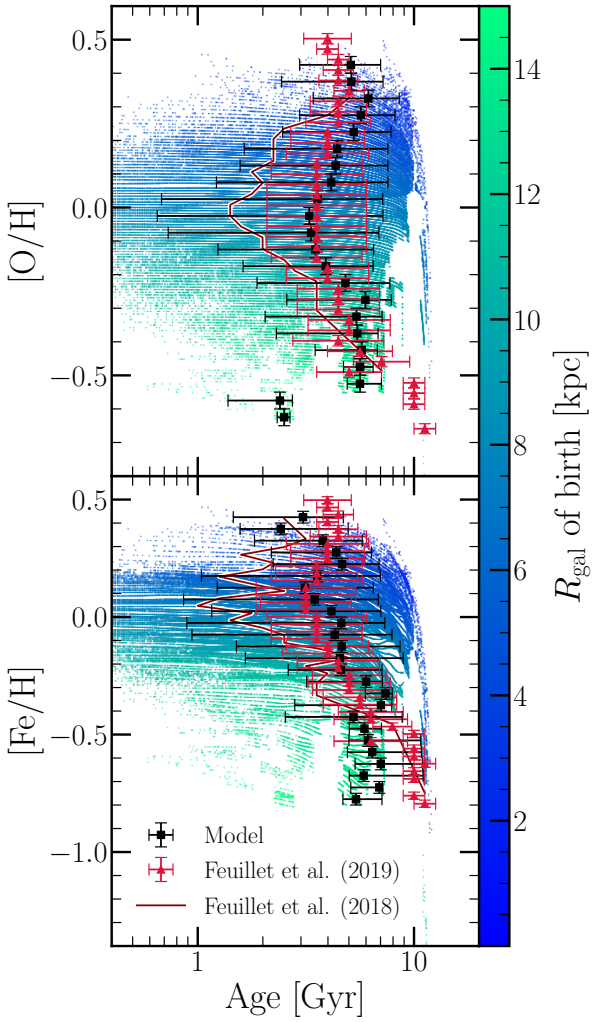

Figure 16. The age-[O/H] (top) and age-[Fe/H] (bottom) relations for the solar annulus (i.e. R_{gal} = 7 - 9 kpc, $|z| \leq 0.5$ kpc) as predicted by our inside-out SFH. Red triangles, black squares, error bars, and background points are as in Fig. 13, but with our simulation prediction quantified in 0.05-dex bins in [O/H] and [Fe/H]. For comparison, we plot the Feuillet et al. (2018) data in a dark red line, omitting the associated uncertainties for the sake of clarity.

age at solar metallicity in both O and Fe (~1 - 2 Gyr as opposed to ~2 - 3 Gyr).

– Fiducial, inside-out SFH performs decently at explaining the Feuillet et al. (2019) AMR, but the ages at solar metallicity in the Feuillet et al. (2018) study are too young for this model. Comparing the black points in this figure to those in Fig. 15 suggests that the constant SFR model can't explain ages that young either. If we were to take the Feuillet et al. (2018) results at face value in comparison to these models, this would strongly suggest a recent enhancement at least in the local star formation rate of the solar annulus to increase the frequency of ~1 Gyr old, solar metallicity stars close to the sun.

– Such a burst is indeed supported by the findings of Mor et al. (2019), who find a factor of ~2 enhancement in the SFH of the Milky Way ~2 Gyr ago by comparing population synthesis models to observed stellar luminosity functions and color-magnitude diagrams with Gaia data (Gaia Collaboration et al. 2018). Isern (2019) reach similar conclusions modeling white dwarf luminosity functions in the solar neighborhood with Gaia parallaxes.

• Fig. 17 shows a comparison of the predicted age-[Fe/H] relation for $|z| \leq 0.5$ kpc stars in the R_{gal} = 5 - 7, 7 - 9, 9 - 11, and 11 - 13 kpc annuli. Points are plotted in the same manner as in Fig. 15 and Fig. 16 in this section.

– Beyond the solar annuulus, we note that our inside-out SFH model in general overpredicts the characteristic ages of stars compared to Feuillet et al. (2019) except for [Fe/H] ≈ +0.4 and -0.5. We also remark that in the trend is not very well reproduced either, particularly in the R_{gal} = 5 - 7 kpc bin.

– In the bottom row of panels, we show the same relation for our late-burst SFH. Interestingly, the late-burst model improves upon the failures of the inside-out model significantly. In particular, the over-prediction of ages of solar and intermediate metallicity stars is fixed by the late-burst model.

· In our recent starburst models, `VICE` calculates that there is a significant amount of low metallicity gas infall required to sustain such an increase in star formation under our adopted $\dot{\Sigma}_\star - \Sigma_g$ relation (see bottom two panels of Fig. 4 and § 2.5).

· Denoting the ages and compositions of the individual stellar populations from our simulations, the colored points in the background of these panels trace the metallicity of the gas as a function of time at various radii. That is, the blue points also represent the [Fe/H] of the gas phase at small radii at various lookback times, and the same for the green points and large radii.

· This demonstrates that at a lookback time of ~2 Gyr, by construction, the ISM at nearly all Galactocentric radii decreased in metallicity. At the same time, the star formation rates increased by a factor of ~2, again by construction (see the right-hand panels of Fig. 4). The result is that at any radius, the frequency of $-0.5 \lesssim$ [O/H] $\lesssim 0$ stars at ages of ~2 Gyr is increases by a factor of ~2 from the inside-out model, decreasing the characteristic ages of stars at these metallicities.

· Although there appears to be an offset between the Feuillet et al. (2019) data and our predicted AMR at high R_{gal}, the late-burst model describes the observed trend noticeably better than the inside-out model. Although the ages of modestly sub-solar metallicity stars in the solar annulus are slightly under-predicted by the model, the same can be said about the trend here and at 5 - 7 kpc as well.

· The parameters which control this offset are the yields of Fe and the mass-loading factor as a function of R_{gal}. If we were to take a slightly higher yield of Fe, it would however increase the overall normalization at $R_{gal} < 9$ kpc as well, where we do not see this discrepancy. It's possible that the mass-loading factor η (see discussion in §2.3) increases too quickly at large R_{gal} in our models, or that outflows are more efficient at removing individual elements from the star forming reservoir. Variable metal-loading factors η_Z would be supported by the observations of Chisholm, Tremonti & Leitherer (2018).

· We remark that the late-burst model predicts extremely young characteristic ages for the highest [Fe/H] bins in the 5 - 7 kpc annulus. This is merely a consequence of the re-enrichment that accompanies the ensuing starburst; in infall-driven starbursts such as this, the abundances often reach

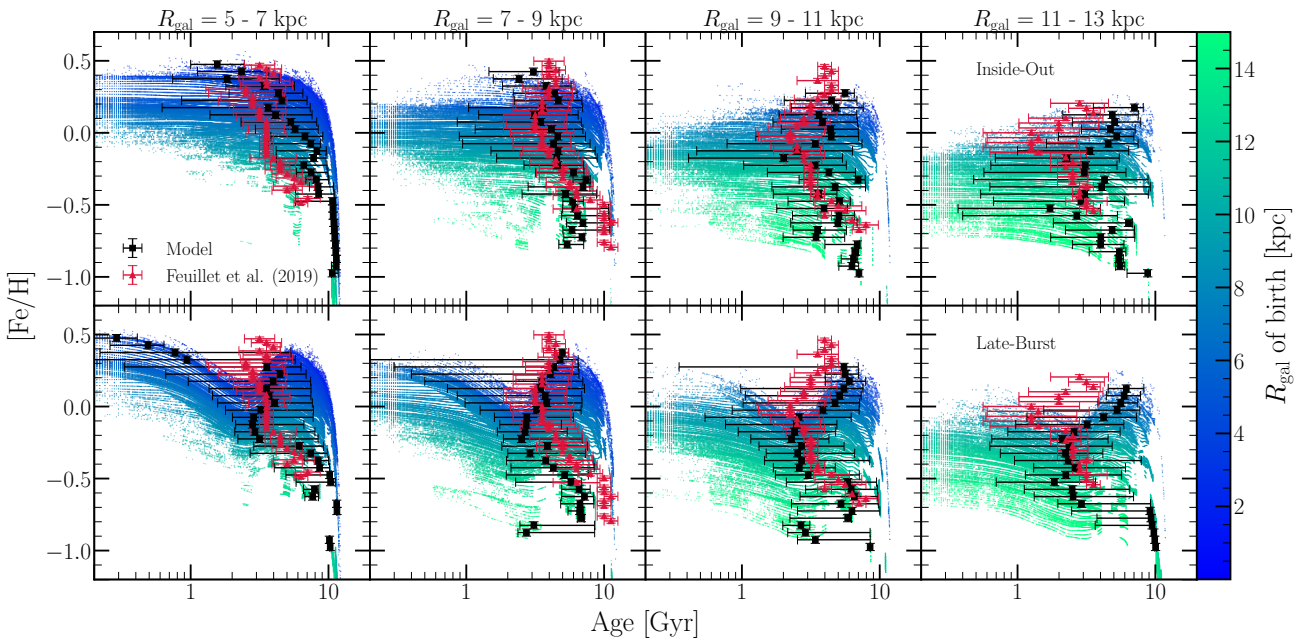

Figure 17. The age-[Fe/H] relation predicted by our inside-out (top) and late-burst (bottom) SFHs for R_{gal} = 5 - 7 kpc (left), 7 - 9 kpc (left middle), 9 - 11 kpc (right middle), and 11 - 13 kpc (right). Each panel plots only the $|z| \leq 0.5$ kpc population. Red triangles, black squares, error bars, and background points are as in Fig. 13 for the corresponding Galactic region, but with our simulation prediction quantified in 0.05-dex bins in [Fe/H].

super-equilibrium values while the star formation rate is still perturbed, which then decay together back to their pre-burst, equilibrium values (Johnson & Weinberg 2020). On Fig. 17, this is noticeable by the abundances on the left-hand edge of each panel being higher in the late-burst scenario. The points that we have plotted as characteristic ages represent that 50th percentile of the mass-weighted age distribution of our stellar populations in a bin of abundance; in other words, a mass-weighted *median*. The age-distribution at these abundances is bimodal, noticeable by the colored points in the background, indicating that the median may not be the best statistic for these few stellar populations. We note that the outer-burst model, in which R_{gal} < 6kpc do not experience the starburst, does not suffer from this issue. The minutia of the AMR at different radii in our late starburst models is sensitive to the detailed time-dependence of the straburst in each annulus.

• Conclude that the AMR reported by Feuillet et al. (2019) is better described by our late starburst models than the inside-out model. This is at odds with our findings in the same simulations with the same observational dataset with regard to the age-[α/Fe] relation. Perhaps the differences can be reconciled.

– The models would be able to have their cake and eat it too if there is a recent starburst with no ensuing α-enhancement. This is difficult to rationalize, however, because an increase in [α/Fe] in the wake of a starburst is a direct consequence of the perturbed ratio of CCSN-SN Ia rates caused by the burst (Johnson & Weinberg 2020). We argue based on this that it is unlikely that the detailed timing of a recent starburst would mitigate this issue.

– It's possible that the Milky Way experienced dilution with no ensuing starburst. This could be the case if the accreted gas was mostly in the form of HI or HII that has not yet cooled and been available for star formation, but has been mixing with the nucleosynthetic products of ongoing star formation in the Galaxy. With dilution playing a noticeable role in the AMR predicted by our burst models, it's possible a model of this nature could agree with both the AMR and the age-[α/Fe] relation. This would require future studies which include a treatment of a multi-phase ISM. This would however be at odds with the findings of Mor et al. (2019) and Isern (2019).

• As a general result here, we caution future studies against leveraging the agreement between a chemical evolution model and observational data based on the solar annulus alone. Fig. 16 presents the comparison of our fiducial, inside-out SFH model predictions in the solar annulus to the Feuillet et al. (2019) data, and Fig. 17 compares the inside-out and late-burst predictions in a larger range of radii. Had we only considered the solar annulus, we would have concluded that the fiducial, inside-out model agrees with the Feuillet et al. (2019) data well. However, in considering other regions of the Galaxy, we found that the inside-out model actually had a handful of failures which were mitigated by our late-burst model.

• With our age-[O/H] and age-[Fe/H] relations, we find similar results as in § 3.4 whereby our model in general overpredicts the observed ages of stars at high $|z|$. Discussion of potential sources of this can be found in § 3.4.

4 CONCLUSIONS

• We have modeled the Milky Way as a series of concentric annuli with ΔR_{gal} = 100 pc width, describing each annulus as a conventional one-zone model of chemical evolution, and allowing the exchange of stellar populations between zones to model the impact of stellar migration on enrichment in the Galaxy. Though there have been a number of studies to date with a similar treatment

of the Galaxy (e.g. Matteucci & Francois 1989; Schönrich & Binney 2009; Nidever et al. 2014; Sharma et al. 2020), ours and the Minchev et al. (2013, 2014, 2017) model are the only which make use of hydrodynamical simulation to describe radial mixing, for which we take the h277 zoom-in simulation. This yields a model for migration which does not have any free parameters (see discussion in § 2.1).

- Our model assumes nucleosynthetic yields and a SN Ia DTD based on a combination of theoretical and empirical constrants. The main free parameters are the star formation law ($\tau_\star(R_{\rm gal}, T)$, see § 2.5), the mass-loading factor $\eta(R_{\rm gal})$ (assumed to be time-independent, see § 2.3), and the SFH. The first we choose from the observed $\dot{\Sigma}_\star - \Sigma_{\rm g}$ relation in local spirals. The second is chosen to match the metallicity gradient. The fiducial model then has an inside-out SFH calibrated to the Sánchez (2020) data. We also consider models with a late starburst, motivated by Mor et al. (2019) and Isern (2019), and a constant-SFH model with a theoretical motivation.
- Our model predicts masses and abundances for simple stellar populations, a given number of which form in a given annulus and timestep. From the hydrodynamical simulation, each stellar population finds a star particle from h277 to act as its *analog*, assigned such that it the star particle was born at a similar Galactocentric radius and time. The stellar population in our chemical evolution model then assumes the change in radius $\Delta R_{\rm gal}$ and final height above/below the disc midplane $|z|$ of its analog at face value.
- We demonstrate that the dependence of the number of high- and low-α sequence stars on Galactic region is at least in part a natural consequence of radial migration. In our models, low [Fe/H], high [α/Fe] stars are located at low $R_{\rm gal}$ and high $|z|$; conversely, the high [Fe/H], low [α/Fe] stars are preferentially found at high $R_{\rm gal}$ and low $|z|$. We clarify that this is not an explanation for the *origin* of the two sequences - only the positional dependence thereof.
- We find that migration-induced fluctuations in the SN Ia rate are a significant effect. The characteristic delay time of a SN Ia rate is of order 1 Gyr (Maoz & Mannucci 2012; Maoz & Graur 2017), while stars are migrating a significant distance in the radial direction on similar timescales in our models. The result is a SN Ia rate which, at fixed radius, tends to follow what is expected in a one-zone model with the same SFH, but shows significant variability on ~Gyr timescales. Our model also predicts this variability to grow with increasing radius due to sampling noise having a greater impact where the stellar number density is low.

  – We demonstrate that this is a mechanism with which truly young, high [α/Fe] stars can be formed. In a region of time and space where the SN Ia rate is lower than expected from the SFH, the ISM will become Fe-poor, increasing the gas-phase [α/Fe] ratio on timescales comparable to the local gas depletion time. Stars then form in this region of the ISM, encoding this composition in their atmospheres, and then migrate to the solar annulus, where they're seen in observations as young, super-solar [α/Fe] stars. While there's an observational argument that at least some fraction of these stars are mass transfer events (e.g. Silva Aguirre et al. 2018; Hekker & Johnson 2019), our model suggests that some fraction of the remaining stars are truly young, not α-enhanced but Fe-poor stars.

  – In general, our results are broadly consistent with Kubryk et al. (2013) and Khoperskov et al. (2021), who argue that radial migration has a negligible impact on the [α/Fe]-[Fe/H] distribution over time. While we find significant deviations in the gas-phase tracks between the post-processing and diffusion migration models, the differences in the stellar distributions are not significantly sensitive to this. We argue that radial migration plays a role in establishing scatter in the age-metallicity and age-[α/Fe] relations, but not in the population-averaged trends.

- While our procedure for building in a radial metallicity gradient ensured that the stellar abundances as a function of $R_{\rm gal}$ match observations, we find that the model-predicted stellar [O/Fe] gradient as well as the gas-phase [O/H] and [Fe/H] gradients are sensitive to the that assumption about the SFH. The differences are most noticeable in where there are offsets between the gas and the stellar gradients, and in the case of the [O/Fe] gradient, its shape in the inner Galaxy.
- We find that our model adequately reproduces the differences in MDFs in bins of $R_{\rm gal}$ in the disc. While there is potential for improvement in the $R_{\rm gal}$ = 3 - 5 kpc bin, the model nonetheless performs well. With increasing $|z|$, however, the prediction breaks down somewhat. Where the observational data show a convergence of the MDFs at all radii to a skew-positive distribution with mode [O/H] ≈ mode [Fe/H] ≈ -0.5, our model predicts the mode of the distributions at small $R_{\rm gal}$ to decrease slightly, but not as much as the observations, while those at large $R_{\rm gal}$ remain largely unchanged. While there is an effect of the right sign, our models cannot explain this entirely.
- Our model successfully reproduces the broad nature of the [O/Fe] distributions at fixed [Fe/H] in bins of $R_{\rm gal}$ and $|z|$ as observed in APOGEE (Hayden et al. 2015). The position of the mode of the distribution is generally well-reproduced as well, the exception being at small $R_{\rm gal}$ and high $|z|$; this is, however, the region of the Galaxy with the fewest number of stars in APOGEE. The principle shortcoming of our model in comparison to the observed data is an overpredicted frequency of intermediate [O/Fe] stars. While the model predicts broad [O/Fe] distributions, and in some bins in [Fe/H] and Galactic regions may show a convincing two-peak profile, it does not reproduce the observations in detail. Remark on the discrepancy with Sharma et al. (2020) closer to the end of the conclusion, after going through results as they appear in the text.
- We find that the age-[O/Fe] as reported by Feuillet et al. (2019) is well-fit by our fiducial inside-out SFH model. In the case of our recent starburst models, the global nature of the burst implies an overall increase in the bulk population-averaged [O/Fe] of young stars which simply isn't seen in the data. The inside-out SFH model, on the other hand, predicts a monotonically declining age-[O/Fe] relation as observed.
- Potentially something on the $R_{\rm gal}$ and $|z|$-dependencies of the age-[α/Fe] relation, and/or the larger scatter with increasing $R_{\rm gal}$, the latter pending a comparison to the post-processing migration model. Regardless, the increased scatter might be worth highlighting here; Jennifer tells me that they're still trying to make sense of Jack Warfield's results, and higher scatter in age-[O/Fe] with increasing $R_{\rm gal}$ can explain a lot.
- We find that the AMR (both age-[O/H] and age-[Fe/H]) in the solar annulus is well-described by our fiducial, inside-out SFH model. However, when the comparison is extended to a wider range of Galactocentric radii, there are a number of noticeable shortcomings. Specifically, the model over-predicts the ages of [Fe/H] ≈-0.5 - -0.2 stars at $R_{\rm gal}$ = 5 - 7 kpc, and fails to reproduce the observed trend at nearly all radii. Where it originally failed to accurately describe the observed age-[α/Fe] relation, our late-burst SFH model improves significantly on these failures of the inside-out model; both the over-predicted ages of sub-solar [Fe/H] stars at 5 - 7 kpc and the population-averaged trends favor the late-burst model over the inside-out model.

- Discussion of late-burst vs. inside-out

  – The late-burst model, motivated by observationally inferred recent SFH of the Galaxy, has little impact on MDFs and the overall [O/Fe]-[Fe/H] structure, but impacts the age-[O/Fe] and age-[Fe/H] relations significantly. While it worsens the agreement with the observed age-[O/Fe] relation considerably, it improves it with the age-[Fe/H] also rather strikingly. In general, I would assert based on this that since different observables favor different models for the recent SFH of the Galaxy, that likely means there's some piece of physics that our model isn't capturing. That'd be worth highlighting in the conclusion, because finding where to go look to potentially find new physics is always exciting.

- Discussion of [α/Fe] dichotomy

  – The [O/Fe] distributions predicted by our models are less bimodal than in the observations, and this is true for all of our models. Radial mixing does produce broad [O/Fe] distributions at fixed [Fe/H] in bins of $R_{\rm gal}$ and $|z|$, but with the accretion and SF histories adopted here, there are too many intermediate [α/Fe] stars to describe the data in detail. Specifically, our models fail in such a manner that a two-infall model (e.g. Chiappini et al. 1997, 2001; Romano et al. 2010; Grisoni et al. 2017; Noguchi 2018; Spitoni et al. 2016, 2018, 2019, 2020, 2021) may significantly improve the agreement. Alternative forms of the SFH which do predict a Milky Way-like [α/Fe] bimodality is of particular interest for future work.

  – These findings are at odds with Sharma et al. (2020), who claim to reproduce the dichotomy using only an inside-out SFH and radial migration. In their model, the evolution of the gas-phase [Fe/H] and [O/Fe] are parameterized a priori by assumed parameterized functions of $R_{\rm gal}$ and T which are selected to agree with the observations. This means that the enrichment and star formation histories of their models are not necessarily internally consistent. In `VICE`, the enrichment history is determined from the star formation history via assumptions about the yields and delay-time distributions of nucleosynthetic channels, internally consistent by construction. We therefore contend that the models explored in this paper are the more self-consistent of the two. To be completely honest here, I have no scope for what would be considered too harsh for a paper - my first time in this position. Obviously, the last thing I want to do is anger the Sharma et al. (2020) authors, but this is my honest critique of their paper.

- We remark on the low number of multi-zone chemical evolution models in the literature. We call for more studies which adopt a similar approach; with only a handful of simulations which can be ran in a combined time interval of less than a single working day, we were able to assess model predictions of various chemical evolution scenarios in comparison to a wide range of observables. With a wealth of one-zone chemical evolution models (both numerical and analytic) and high-resolution hydrodynamical simulations already in the literature, there is a true void in the literature for these medium resolution, medium computational expense models which which can teach us a great deal about the enrichment history of the Milky Way. For this reason, `VICE` is open source software, and its `milkyway` object which ran our simulations adopts many of this paper's physically and observationally motivated assumptions as default values. Alternative zone configurations can be achieved by subclassing the `multizone` object and specifying how gas and stars should move between the individual zones, as we have already done for the `milkyway` object.
- `VICE` is publicly available and open-source. It can be installed via `pip` (`https://pypi.org/project/vice`). Documentation is available at `https://vice-astro.readthedocs.io`. Source code is hosted at `https://github.com/giganano/VICE.git`. `Python` code which runs the simulations presented in this paper are included as supplementary material in the `git` repository; our models can be ran directly from a `bash` terminal without modifying the source code, and are capable of predicting abundances for ~2 million stellar populations in only ~2 CPU hours with a single core on personal computers.

5 ACKNOWLEDGEMENTS

We are grateful to Diane Feuillet for sharing the data from Feuillet et al. (2018) and Feuillet et al. (2019) with us. There will be others added, depending on whether or not they go here or on the author's list. I'll also need to add the SDSS acknowledgements since we made use of APOGEE data.

Software: Matplotlib (Hunter 2007); Astropy (Astropy Collaboration et al. 2013, 2018); NumPy (Harris et al. 2020).

6 DATA AVAILABILITY

In case anyone hasn't seen one of these Data Availability statements yet, this is now a requirement by MNRAS. It wasn't when I submitted my last paper, but was by the time we were finished with the referee report, so I wound up having to add one. They just want you to say if the data are available to the reader or not, and where/how they can get it if they are. `VICE` is open source software, and as such the source code for these simulations is publicly available.[2] The source code which produces the outputs presented in this paper as well as the figures are included as secondary material in the GitHub repository. While the aggregate of all outputs analyzed in this paper are sufficiently large that it is not conducive to store them on GitHub, we provide instructions on how to run our simulations and variations thereof. All observational data appearing in this paper is publicly available, and is also included with the source code for our simulations and figures.

[2] `https://pypi.org/project/vice`
`https://vice-astro.readthedocs.io`
`https://github.com/giganano/VICE.git`

Appendices

A NORMALIZING A FIDUCIAL STAR FORMATION HISTORY

• Derive formula for normalizing an SFH given the time-dependence at a given radius $f(t|R_{\rm gal})$ and the radial dependence of the desired surface density gradient at late times $g(R_{\rm gal})$. Neither need be normalized.

$$\dot{\Sigma}_\star(R_{\rm gal}, t) = \dot{\Sigma}_{\star,0}(R_{\rm gal}) f(t|R_{\rm gal}) \tag{20}$$

$$\Sigma_\star(r) = \Sigma_{\star,0} g(R_{\rm gal}) \tag{21}$$

• Integrate surface density of star formation with time and you get the present day surface density gradient at that radius. This yields the unknown $\dot{\Sigma}_{\star,0}$ in terms of $\Sigma_\star(R_{\rm gal})$ and subsequently the unknown $\Sigma_{\star,0}$.

$$\Sigma_\star(R_{\rm gal}) \approx (1-r)\int_0^T \dot{\Sigma}_\star(R_{\rm gal}, t)dt \tag{22a}$$

$$= (1-r)\dot{\Sigma}_{\star,0}(R_{\rm gal})\int_0^T f(t|R_{\rm gal})dt \tag{22b}$$

$$\implies \dot{\Sigma}_{\star,0}(R_{\rm gal}) = \Sigma_\star(R_{\rm gal})\left[(1-r)\int_0^T f(t|R_{\rm gal})dt\right]^{-1} \tag{22c}$$

$$= \Sigma_{\star,0} g(R_{\rm gal})\left[(1-r)\int_0^T f(t|R_{\rm gal})dt\right]^{-1} \tag{22d}$$

• Integrate surface density over area of the disc and you get the present day Milky Way stellar mass. This solves for the unknown $\Sigma_{\star,0}$:

$$M_\star^{\rm MW} = \int_0^R \Sigma_\star(R_{\rm gal}) 2\pi R_{\rm gal} dR_{\rm gal} \tag{23a}$$

$$= \Sigma_{\star,0}\int_0^R g(R_{\rm gal}) 2\pi R_{\rm gal} dR_{\rm gal} \tag{23b}$$

$$\implies \Sigma_{\star,0} = M_\star^{\rm MW}\left[\int_0^R g(R_{\rm gal}) 2\pi R_{\rm gal} dR_{\rm gal}\right]^{-1} \tag{23c}$$

• Combine the last two equations into $\dot{\Sigma}_\star(R_{\rm gal}, t)$ and obtain the following equation:

$$\dot{\Sigma}_\star(R_{\rm gal}, t) = A f(t|R_{\rm gal}) g(R_{\rm gal}) \tag{24}$$

where

$$A = M_\star^{\rm MW}\left[(1-r)\int_0^R g(R_{\rm gal}) 2\pi R_{\rm gal} dR_{\rm gal}\int_0^T f(t|R_{\rm gal})dt\right]^{-1} \tag{25}$$

This result makes intuitive sense: $f(t|R_{\rm gal})$ specifies the time-dependence of the SFH and $g(R_{\rm gal})$ specifies the radial dependence by construction, and $M_\star^{\rm MW}$ sets the overall normalization.

• This recipe implicitly assumes that radial migration does not significantly alter the surface density profile, and we have demonstrated in § 2.6 that this is the case for the Galactocentric radii of interest in this paper. It introduces scatter, but does not alter the overall dependence. This recipe can be employed in disc galaxy models as long as this is not violated.

REFERENCES

Abolfathi B., et al., 2018, ApJS, 235, 42
Adams S. M., Kochanek C. S., Gerke J. R., Stanek K. Z., Dai X., 2017, MNRAS, 468, 4968
Ahumada R., et al., 2020, ApJS, 249, 3
Andrews B. H., Weinberg D. H., Schönrich R., Johnson J. A., 2017, ApJ, 835, 224
Asplund M., Grevesse N., Sauval A. J., Scott P., 2009, ARA&A, 47, 481
Astropy Collaboration et al., 2013, A&A, 558, A33
Astropy Collaboration et al., 2018, AJ, 156, 123
Basinger C. M., Kochanek C. S., Adams S. M., Dai X., Stanek K. Z., 2020, arXiv e-prints, p. arXiv:2007.15658
Berg D. A., Skillman E. D., Croxall K. V., Pogge R. W., Moustakas J., Johnson-Groh M., 2015, ApJ, 806, 16
Berg D. A., Pogge R. W., Skillman E. D., Croxall K. V., Moustakas J., Rogers N. S. J., Sun J., 2020, ApJ, 893, 96
Bigiel F., Leroy A., Walter F., Blitz L., Brinks E., de Blok W. J. G., Madore B., 2010, AJ, 140, 1194
Bird J. C., Kazantzidis S., Weinberg D. H., Guedes J., Callegari S., Mayer L., Madau P., 2013, ApJ, 773, 43
Bird J. C., Loebman S. R., Weinberg D. H., Brooks A., Quinn T. R., Christensen C. R., 2020, arXiv e-prints, p. arXiv:2005.12948
Bland-Hawthorn J., Gerhard O., 2016, ARA&A, 54, 529
Brooks A. M., Zolotov A., 2014, ApJ, 786, 87
Brown J. S., et al., 2019, MNRAS, 484, 3785
Buck T., 2020, MNRAS, 491, 5435
Buck T., Obreja A., Macciò A. V., Minchev I., Dutton A. A., Ostriker J. P., 2020, MNRAS, 491, 3461
Chiappini C., Matteucci F., Gratton R., 1997, ApJ, 477, 765
Chiappini C., Matteucci F., Romano D., 2001, ApJ, 554, 1044
Chiappini C., et al., 2015, A&A, 576, L12
Chieffi A., Limongi M., 2004, ApJ, 608, 405
Chieffi A., Limongi M., 2013, ApJ, 764, 21
Chisholm J., Tremonti C., Leitherer C., 2018, MNRAS, 481, 1690
Christensen C., Quinn T., Governato F., Stilp A., Shen S., Wadsley J., 2012, MNRAS, 425, 3058
Clarke A. J., et al., 2019, MNRAS, 484, 3476
Cristallo S., et al., 2011, ApJS, 197, 17
Daflon S., Cunha K., de la Reza R., Holtzman J., Chiappini C., 2009, AJ, 138, 1577
de los Reyes M. A. C., Kennicutt Robert C. J., 2019, ApJ, 872, 16
Edvardsson B., Andersen J., Gustafsson B., Lambert D. L., Nissen P. E., Tomkin J., 1993, A&A, 500, 391
Ellison S. L., Lin L., Thorp M. D., Pan H.-A., Scudder J. M., Sanchez S. F., Bluck A. F. L., Maiolino R., 2020a, arXiv e-prints, p. arXiv:2012.04771
Ellison S. L., Lin L., Thorp M. D., Pan H.-A., Sanchez S. F., Bluck A. F. L., Belfiore F., 2020b, arXiv e-prints, p. arXiv:2012.04772
Feuillet D. K., et al., 2018, Monthly Notices of the Royal Astronomical Society, 477, 2326
Feuillet D. K., Frankel N., Lind K., Frinchaboy P. M., García-Hernández D. A., Lane R. R., Nitschelm C., Roman-Lopes A. r., 2019, MNRAS, 489, 1742
Frankel N., Rix H.-W., Ting Y.-S., Ness M., Hogg D. W., 2018, ApJ, 865, 96
Frankel N., Sanders J., Ting Y.-S., Rix H.-W., 2020, ApJ, 896, 15
Fraternali F., Tomassetti M., 2012, MNRAS, 426, 2166
Frinchaboy P. M., et al., 2013, ApJ, 777, L1
Gaia Collaboration et al., 2018, A&A, 616, A1
García-Benito R., et al., 2017, A&A, 608, A27
García Pérez A. E., et al., 2016, AJ, 151, 144
Gerke J. R., Kochanek C. S., Stanek K. Z., 2015, MNRAS, 450, 3289
González Delgado R. M., et al., 2014, A&A, 562, A47
Grand R. J. J., et al., 2017, MNRAS, 467, 179
Grand R. J. J., et al., 2018, MNRAS, 474, 3629
Griffith E., et al., 2020, arXiv e-prints, p. arXiv:2009.05063
Grisoni V., Spitoni E., Matteucci F., Recio-Blanco A., de Laverny P., Hayden M., Mikolaitis Ŝ., Worley C. C., 2017, MNRAS, 472, 3637

Harris C. R., et al., 2020, Nature, 585, 357
Hayden M. R., et al., 2014, AJ, 147, 116
Hayden M. R., et al., 2015, ApJ, 808, 132
Haywood M., 2008, MNRAS, 388, 1175
Hekker S., Johnson J. A., 2019, MNRAS, 487, 4343
Holmberg J., Nordström B., Andersen J., 2007, A&A, 475, 519
Holoien T. W. S., et al., 2019, MNRAS, 484, 1899
Holtzman J. A., et al., 2015, AJ, 150, 148
Hunter J. D., 2007, Computing in Science & Engineering, 9, 90
Isern J., 2019, ApJ, 878, L11
Johnson J. W., Weinberg D. H., 2020, MNRAS, 498, 1364
Kennicutt Robert C. J., 1998, ApJ, 498, 541
Kennicutt R. C., Evans N. J., 2012, ARA&A, 50, 531
Kennicutt Robert C. J., de los Reyes M. A. C., 2020, arXiv e-prints, p. arXiv:2012.05363
Khoperskov S., Haywood M., Snaith O., Di Matteo P., Lehnert M., Vasiliev E., Naroenkov S., Berczik P., 2021, MNRAS, 501, 5176
Kroupa P., 2001, MNRAS, 322, 231
Krumholz M. R., Burkhart B., Forbes J. C., Crocker R. M., 2018, MNRAS, 477, 2716
Kubryk M., Prantzos N., Athanassoula E., 2013, MNRAS, 436, 1479
Leroy A. K., Walter F., Brinks E., Bigiel F., de Blok W. J. G., Madore B., Thornley M. D., 2008, AJ, 136, 2782
Leroy A. K., et al., 2013, AJ, 146, 19
Licquia T. C., Newman J. A., 2015, ApJ, 806, 96
Liu L., Gao Y., Greve T. R., 2015, ApJ, 805, 31
Loebman S. R., Ivezić Ž., Quinn T. R., Governato F., Brooks A. M., Christensen C. R., Jurić M., 2012, ApJ, 758, L23
Loebman S. R., et al., 2014, ApJ, 794, 151
Majewski S. R., et al., 2017, AJ, 154, 94
Maoz D., Graur O., 2017, ApJ, 848, 25
Maoz D., Mannucci F., 2012, Publ. Astron. Soc. Australia, 29, 447
Martig M., et al., 2016, MNRAS, 456, 3655
Matteucci F., Francois P., 1989, MNRAS, 239, 885
Melioli C., Brighenti F., D'Ercole A., de Gouveia Dal Pino E. M., 2008, MNRAS, 388, 573
Melioli C., Brighenti F., D'Ercole A., de Gouveia Dal Pino E. M., 2009, MNRAS, 399, 1089
Minchev I., Chiappini C., Martig M., 2013, A&A, 558, A9
Minchev I., Chiappini C., Martig M., 2014, A&A, 572, A92
Minchev I., Steinmetz M., Chiappini C., Martig M., Anders F., Matijevic G., de Jong R. S., 2017, ApJ, 834, 27
Mor R., Robin A. C., Figueras F., Roca-Fàbrega S., Luri X., 2019, A&A, 624, L1
Navarro J. F., Frenk C. S., White S. D. M., 1997, ApJ, 490, 493
Nidever D. L., et al., 2014, ApJ, 796, 38
Noguchi M., 2018, Nature, 559, 585
Nordström B., Andersen J., Holmberg J., Jørgensen B. R., Mayor M., Pont F., 2004a, Publ. Astron. Soc. Australia, 21, 129
Nordström B., et al., 2004b, A&A, 418, 989
Peek J. E. G., 2009, ApJ, 698, 1429
Pejcha O., Thompson T. A., 2015, ApJ, 801, 90
Pinsonneault M. H., et al., 2014, ApJS, 215, 19
Radburn-Smith D. J., et al., 2012, ApJ, 753, 138
Recio-Blanco A., et al., 2014, A&A, 567, A5
Rojas-Arriagada A., et al., 2017, A&A, 601, A140
Romano D., Karakas A. I., Tosi M., Matteucci F., 2010, A&A, 522, A32
Roškar R., Debattista V. P., Stinson G. S., Quinn T. R., Kaufmann T., Wadsley J., 2008a, ApJ, 675, L65
Roškar R., Debattista V. P., Quinn T. R., Stinson G. S., Wadsley J., 2008b, ApJ, 684, L79
Ruiz-Lara T., Gallart C., Bernard E. J., Cassisi S., 2020, Nature Astronomy, 4, 965
Sánchez S. F., 2020, ARA&A, 58, 99
Schönrich R., Binney J., 2009, MNRAS, 396, 203
Sellwood J. A., Binney J. J., 2002, MNRAS, 336, 785
Sharma S., Hayden M. R., Bland-Hawthorn J., 2020, arXiv e-prints, p. arXiv:2005.03646
Silva Aguirre V., et al., 2018, MNRAS, 475, 5487
Spitoni E., Recchi S., Matteucci F., 2008, A&A, 484, 743
Spitoni E., Matteucci F., Recchi S., Cescutti G., Pipino A., 2009, A&A, 504, 87
Spitoni E., Vincenzo F., Matteucci F., Romano D., 2016, MNRAS, 458, 2541
Spitoni E., Matteucci F., Jönsson H., Ryde N., Romano D., 2018, A&A, 612, A16
Spitoni E., Silva Aguirre V., Matteucci F., Calura F., Grisoni V., 2019, A&A, 623, A60
Spitoni E., Verma K., Silva Aguirre V., Calura F., 2020, A&A, 635, A58
Spitoni E., et al., 2021, arXiv e-prints, p. arXiv:2101.08803
Sukhbold T., Ertl T., Woosley S. E., Brown J. M., Janka H. T., 2016, ApJ, 821, 38
Tacconi L. J., et al., 2018, ApJ, 853, 179
Vincenzo F., Kobayashi C., 2020, MNRAS, 496, 80
Vincenzo F., Weinberg D. H., Miglio A., Lane R. R., Roman-Lopes A., 2021, arXiv e-prints, p. arXiv:2101.04488
Wadsley J. W., Keller B. W., Quinn T. R., 2017, MNRAS, 471, 2357
Wang L., Dutton A. A., Stinson G. S., Macciò A. V., Penzo C., Kang X., Keller B. W., Wadsley J., 2015, MNRAS, 454, 83
Weinberg D. H., Andrews B. H., Freudenburg J., 2017, ApJ, 837, 183
Weinberg D. H., et al., 2019, ApJ, 874, 102
Wielen R., Fuchs B., Dettbarn C., 1996, A&A, 314, 438
Zolotov A., et al., 2012, ApJ, 761, 71